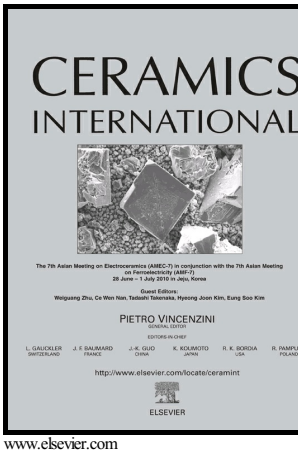

Research progress on iron oxide-based magnetic materials: Synthesis techniques and photocatalytic applications

Yean Ling Pang, Steven Lim, Hwai Chyuan Ong, Wen Tong Chong

PII: S0272-8842(15)01670-3
DOI: http://dx.doi.org/10.1016/j.ceramint.2015.08.144
Reference: CERI11241

To appear in: *Ceramics International*

Received date: 3 July 2015
Revised date: 14 August 2015
Accepted date: 26 August 2015

Cite this article as: Yean Ling Pang, Steven Lim, Hwai Chyuan Ong and Wer Tong Chong, Research progress on iron oxide-based magnetic materials Synthesis techniques and photocatalytic applications, *Ceramics Internationa* http://dx.doi.org/10.1016/j.ceramint.2015.08.144

Research progress on iron oxide-based magnetic materials: Synthesis techniques and photocatalytic applications

Yean Ling Pang[a,b]*, Steven Lim[a,b], Hwai Chyuan Ong[b] and Wen Tong Chong[b]

[a] Department of Chemical Engineering, Lee Kong Chian Faculty of Engineering and Science,

Universiti Tunku Abdul Rahman, Jalan Sungai Long, Bandar Sungai Long, Cheras 43000 Kajang, Selangor, Malaysia

[b] Department of Mechanical Engineering, Faculty of Engineering,

University of Malaya, 50603 Kuala Lumpur, Malaysia

Tel: +603-9086 0288 Fax: +603-9019 8868

*E-mail: pangyl@utar.edu.my; pangyeanling@hotmail.com

Abstract

Heterogeneous photocatalysis is a promising strategy for advanced oxidation environmental remediation. Herein, this review aims to highlight recent development in the preparation of iron oxide-based magnetic nanoparticles and their applications for photocatalytic removal of organic pollutants in aqueous solution. The usage of iron oxide-based magnetic photocatalysts has received considerable attention in recent years due to their unique properties such as excellent magnetic properties, high stability against corrosion, large surface area and high surface modification flexibility. The synthesis routes for iron oxide nanomaterials such as co-precipitation, thermal decomposition, solvothermal, hydrothermal and microelmulsion processes had been summarized. Recent advances on the surface modification of iron oxide incorporating

impurity doping, metal-loading, composite semiconductors and encapsulation of iron oxide are reviewed. In addition, the effect of surface modified iron oxide-based materials on the photocatalytic degradation performance and photocatalytic reaction mechanism are discussed in detail. Lastly, the toxicological effects owing to the iron oxide-based magnetic nanoparticles and potential challenges on their application in a sustainable way are also discussed.

Keywords: Photocatalysis; iron oxide; magnetic; modification; mechanism

1. Introduction

Photocatalysts utilize light energy to carry out oxidation and reduction reactions. During photocatalytic oxidation, photocatalyst absorbs light energy and excites electron from the valence band into the conduction band. The resulting electron and hole can then further react with oxygen (O_2) and water (H_2O) to form superoxide anion (O_2^-) and hydroxyl radical (•OH), respectively [1]. These two species possess strong oxidizing capability to oxidize organic pollutants. Until now, the most commonly used semiconductor as photocatalyst for degradation of organic pollutants are titanium dioxide (TiO_2) and zinc oxide (ZnO). The major drawback for these photocatalysts is related to its relatively wide band gap energy, i.e. 3.2 eV for anatase TiO_2 [2], 3.02 eV for rutile TiO_2 [3] and 3.2 eV for ZnO [1]. These semiconductors can only be excited by photons which are close to the UV region and utilize only 4–6% of solar light, which limits their practical applications [4].

In order to promote more efficient utilization of solar light, the development of visible light active or narrow band gap semiconductors as photocatalyts has attracted

extensive attention. In this context, iron oxide with appropriate valence state and chemical composition can be considered as a high promising photocatalyst owing to its narrow band gap energy [5], high chemical stability [6], superior stability against corrosion [5] and low toxicity. It has been reported that iron oxide could absorb and utilize about 40 % of the incident solar spectra [2]. However, its photocatalytic efficiency still depends on other factors such as particle size, aggregate size in suspension, crystalline phase, crystallinity and other structural parameters [7].

The separation of photocatalysts from treated water by using centrifugation or filtration is a time consuming and expensive process. This factor restricted the application of suspended photocatalysts in industrial scale. In order to overcome this deficiency, immobilizing photocatalysts on a suitable support has been developed. However, an obvious disadvantage of the immobilization system is the limitation of mass transfer rate [8]. Consequently, suspended system has generally received more attention in the literature. It should be noted that the catalyst surface is only active if the catalyst particle is illuminated. The particles in both suspended and immobilized systems which are further away from the light source may be shielded from the radiation by those near the light source [9, 10]. This will decrease their photocatalytic efficiency.

Magnetic separation technology is a convenient approach for separation and recycle of catalyst. The technology utilizing superconducting high gradient magnetic field has been successfully applied in various industries field such as steel mill industry and water purification plant [11, 12]. Hence, magnetic particles which possess both magnetic and photocatalytic properties have been attracting increasing attention in recent years. The key factor for preparation of magnetic photocatalysts is that they must be stable during the reaction under light irradiation. Photoreactor with

photocatalysts in suspension might suffer limited depth of light incident penetration due to the light blockage (shading effect [13]) or scattering by the catalyst particles. Yet, most of the research works in wastewater tend to coincide that fine particles exhibit higher catalytic activity compared to immobilized catalyst [8]. Efforts on combining other treatment technologies such as acoustic cavitation will help in minimizing shading effect encountered during photocatalysis [13]. However, this is not the focus in this review.

Various methods to synthesize magnetic iron oxide nanoparticles such as co-precipitation of Fe ions in alkaline solutions [14, 15], thermal decomposition of iron precursor in organic solution [16], hydrothermal [17], solvothermal [18] and microemulsion [19] have been reported in the literature. All the methods have been investigated to synthesize particles with small size distribution and homogeneous composition. The methods differ in terms of underlying principle, practicality and cost of the necessary equipment. Iron oxide can be obtained in several phases such as hematite (α-Fe_2O_3), maghemite (γ-Fe_2O_3), and magnetite (Fe_3O_4, $Fe(II)Fe(III)_2O_4$), depending upon the synthesis method and conditions. This review is focussed on these three forms of iron oxides since they are the most commonly obtained phases through synthesis procedures.

Hydrophobic surface of iron oxide particles will result in hydrophobic interactions between particles which in turn will cause the agglomeration of particles to form large clusters and reduce the effective surface area [20]. In order to prevent these limitations, magnetic particles are usually coated with the shell of an organic material such as surfactant and polymer [21] to enhance the particles dispersion. Meanwhile, the coating with inorganic material such as silica (SiO_2), carbon and polymer [8, 22] can protect the magnetic particles from un-wanted degradation

influenced by outside environment. The possible chemical degradations are dissolution in acidic media or oxidation of Fe_3O_4 under aerobic conditions. This coated surface can be further functionalized by the attachment of various active molecules to stabilize the nanoparticles in specific conditions and enable different applications.

In addition, pure iron oxide exhibits a miserably short excited state lifetime, a short hole diffusion length and high recombination rate of photo-generated electron-hole pairs [5]. The development of various dimensional nanostructures of iron oxide has been attracting a great interest among scientific researchers due to their unique properties and potential applications in various fields. It is believed that these nanostructures are able to enhance visible light absorption, charge separation and photochemical stability [23]. To date, most of the magnetic photocatalysts have dual components which are magnetic component and photocatalytic component with a photocatalytic function. Numerous efforts have been focused to improve the photocatalytic activity of iron oxide magnetic particles such as doping of various metal or non-metal ions, incorporating noble metals as well as fabricating composites with other photocatalysts to generate magnetic photocatalytic heterostructures. These heterostructures could offer synergetic enhancement to the catalytic activity due to the suppressed recombination rate and promoted transportation rate of photo-generated charge carriers [5].

The goal of this review is to explore the potential of iron oxide as photocatalyst in the environmental wastewater purification. The recent development strategies in the preparation of iron oxide as magnetic photocatalyst, various surface functionalized strategies and their corresponding applications to degrade organic compounds are

scrutinized. Besides, the potential problems and challenges for the application of magnetic iron oxide in photocatalysis are also discussed.

2. Background of iron oxide magnetic particles

Iron oxide can exists in several forms such as iron(II) oxide (FeO), amorphous hydrous ferric oxide (FeOOH), goethite (α-FeOOH), lepidocrocite (γ-FeOOH), Fe_3O_4 (a mixture of Fe(II) and Fe(III)) and iron(III) oxide (Fe_2O_3) phases such as α-Fe_2O_3 and γ-Fe_2O_3 [24]. Although the amorphous FeOOH, α-FeOOH and γ-FeOOH have high surface area which is beneficial to the adsorption process, they are not stable and could easily decompose or form low surface-area crystalline iron oxides during the synthesis and usage [25].

The crystal structures of α-Fe_2O_3, Fe_3O_4 and γ-Fe_2O_3 are shown in Fig. 1 [26]. In α-Fe_2O_3, oxygen atoms are in a hexagonal close-packed arrangement with Fe^{3+} ions occupying two of every three octahedral sites and have no periodic vacancies [27]. In Fe_3O_4, oxygen atoms are in a cubic close-packed arrangement with chemical formula of $(Fe^{3+})_{tetrahedral}[Fe^{2+}Fe^{3+}]_{octahedral}O_4$ and has an inverse spinel structure [28]. γ-Fe_2O_3 has the same crystal structure as Fe_3O_4, with the main difference that γ-Fe_2O_3 has only Fe^{3+} cations and vacancies in their sub-lattices [14]. Each formation has different magnetic behaviors which originating from their vacancies and valance states of irons in sub-lattices [28]. These influence the value of saturation magnetization for bulk α-Fe_2O_3 (65 emu/g), γ-Fe_2O_3 (76 emu/g) and Fe_3O_4 (92 emu/g) [29]. Meanwhile, α-Fe_2O_3 exhibits an extremely high coercivity (H_c > 4000 Oe) as compared to γ-Fe_2O_3 and Fe_3O_4 [30].

The interaction among Fe ions on adjoining sites is the most important attribute to determine the electron spinnings in parallel or non-parallel alignment [31]. Among three types of iron oxide, Fe_3O_4 often shows the highest saturation magnetization due to the electron delocalization can take place between adjacent site of both Fe^{2+} and Fe^{3+}. Fe_3O_4 is known to be unstable under oxidizing conditions (H_2O_2, O_2) [32]. Fe_3O_4 can be transformed to γ-Fe_2O_3 or α-Fe_2O_3 at higher temperatures [32]. Then, Fe_3O_4 can be formed back through hydrogen reduction of α-Fe_2O_3.

Previous book chapter devoted by Liu [33] focuses only on the fabrication of spinel ferrites type of iron oxide due to the ferrimagnetic behavior which possesses high magnetic susceptibility. Although α-Fe_2O_3 exhibits weak ferromagnetic or antiferromagnetic, its contribution to the magnetization and as magnetic photocatalysts should not be ignored. Hence, this review reports on the most recent experimental studies and developments specifically for α-Fe_2O_3, γ-Fe_2O_3 and Fe_3O_4 and their applications as magnetic photocatalysts.

2.1 Magnetic properties of iron oxide

Magnetism arises from the relative motion of electric charge (orbital/spin motion) [34]. It is used to characterise the magnetic phase of materials. Most chemical elements carry an atomic moment in the atomic ground state, while only oxygen, chromium, iron, manganese, cobalt, nickel and some rare earth elements show magnetic ordering in polyatomic state [35]. The fundamental source of material magnetism is magnetic moments, which attributed to the unpaired electrons in their atomic shells especially in the 3d and 4f shells of each atom [36]. Thus, magnetic

moment of delocalized electrons in metals and interatomic interactions between localized magnetic moments in molecules can result in magnetic ordering.

The magnetic moment of an atom arise as a result of interactions between the spin moment of the electron and the orbital moment, where the latter contribution is relatively minor importance [31]. Both the calculated and measured magnetic moments of high spin Fe^{3+} with five unpaired electrons are 5.9 Bohr magnetons due to its zero orbital moment. Meanwhile, the measured magnetic moment (5.1 to 5.5 Bohr magnetons) of Fe^{2+} is different from the calculated value (4.9 Bohr magnetons) indicating the contribution from the orbital moment [37].

Magnetic nanoparticles have been synthesized in different compositions and phases such as pure metals (i.e. Fe, Co, Ni), alloys (i.e. FePt, $FePt_3$, $CoPt_3$), metal oxides or spinel ferrites type with the general formula of MFe_2O_4, where M is a divalent metal cation ($NiFe_2O_4$, $CoFe_2O_4$, $Zn_{0.35}Ni_{0.65}Fe_2O_4$, $MnFe_2O_4$, $MgFe_2O_4$) [24, 32]. Although pure metals such as Fe, Co, Ni possess the highest magnetization saturation, they receive little interest due to their high characteristic toxicity and extremely sensitive to oxidation [38]. In contrast, iron oxides are less sensitive to oxidation and are able to give a stable magnetic response.

Magnetism can be classified by their response to an externally applied magnetic field into five main types: diamagnetism, antiferromagnetism, ferromagnetism, ferrimagnetism and paramagnetism [31, 36]. Different forms of magnetism possess different orientations of magnetic moments. It should be noted that all substances exhibit intrinsic property of weak diamagnetism and they may possess other forms of more significant magnetic behavior. Materials with diamagnetism property are due to the presence of filled electronic subshells, where magnetic moments are paired and

cancelled out each other. In the case of diamagnetism, the interaction is weakly repulsive from a magnetic pole.

Ferromagnetism materials have aligned atomic magnetic moments with equal magnitude and produce large net magnetic moment, thereby; the interaction is strongly attractive towards magnetic pole. Meanwhile, materials having atomic magnetic moments of equal magnitude that are arranged in an anti-parallel fashion and produce no net magnetic moment display antiferromagnetism. The interaction in antiferromagnetism material is strongly repulsive from a magnetic pole. Besides, materials will exhibit paramagnetic behavior when thermal energy is sufficient to cause the equal and oppositely aligned atomic moments to fluctuate randomly. In case of paramagnetism, the interaction is weakly attractive towards magnetic pole. On the other hand, materials that possess different strengths of magnetic moments that arranged in an anti-parallel fashion and produce net magnetic moment exhibited behavior of ferrimagnetism. The interaction in ferrimagnetism material is strongly attractive towards magnetic pole.

Phenomenon of superparamagnetism arises when the size of a particle becomes small enough to exhibit single domain and the magnetic moment fluctuate in random direction because of thermal agitation [39]. Fig. 2 shows the magnetization behavior of ferromagnetic and superparamagnetic nanoparticles under an external magnetic field [36]. The magnetic moment of the domains of ferromagnetic nanoparticle and single-domain superparamagnetic nanoparticles are aligned with the applied field. In the absence of external magnetic field, ferromagnetic nanoparticles maintain a net magnetization while superparamagnetic nanoparticles exhibit no net magnetization due to rapid reversal of the magnetic moment. Thus, the term superparamagnetism

also refers to characteristic strong paramagnetic nature, but with the magnetic moment tends to align with the magnetic field.

2.2 Basic concepts and characterizations of iron oxide magnetic particles

Magnetic properties of nanoparticles are strongly influenced by finite size effects and surface effects [35]. Finite size effects are resulted from the quantum confinement of electrons, while surface effects are related to the symmetry breaking of crystal structure at the boundary of each particle. Further detailed issues has been addressed by Lu et al. [32]. A particle below a critical particle size would consist of a single magnetic domain. A single domain particle has a net magnetic moment that results from the sum of all uncompensated spins in the nanoparticle [24]. Hence, the particles in the range of nanometer size always fall into a single domain due to the exhibition of superparamagnetism properties. For instance, the superparamagnetic properties were observed for α-Fe_2O_3, γ-Fe_2O_3 and Fe_3O_4 with diameters smaller than 20 nm [40], 10 nm [41] and 6 nm [41], respectively.

Magnetic properties of magnetic particles can be described by the induced magnetization (M) on the applied magnetic field (H) [42]. The magnetization directions of magnetic particles are aligned along the magnetic field direction to achieve saturation of magnetization (M_s). The ease at which magnetic particles can be aligned is measured by its susceptibility where it can be described as the ratio of M to H. Meanwhile, magnetic particles could retain their magnetization direction after reduction of the field strength and have a remanent magnetization (M_r) at zero magnetic field strength.

Magnetic permeability can be defined as the tendency of the magnetic lines of force to pass through a medium relative to their tendency to pass through a vacuum [37]. This is the parameter used to distinguish between diamagnetic and paramagnetic materials. The field strength required to demagnetize magnetic material to zero is defined as coercivity (H_c). Magnet with high coercivity is expressed as hard material which has permanent magnetization and not easily demagnetized. Coercivity is strongly size-dependent as shown in Fig. 3 [36]. It has been found that the coercivity increases to a maximum as the particles size is reduced and then decreases toward zero. Besides, particles will change from multi-domain to single-domain when the size of particles is decreased [39].

According to the Curie-Weiss law, the ordered arrangement of magnetic moments decreases with increasing temperature due to thermal fluctuations of the individual moments. The transition temperatures are named as Curie temperature (T_C) for ferromagnetic and ferrimagnetic materials while Néel temperature (T_N) is defined for antiferromagnetic materials. For example, α-Fe_2O_3 has T_C of 956 K, γ-Fe_2O_3 has T_N of 820–986 K and Fe_3O_4 has 850 K [41]. Below the transition temperature, compounds may undergo transition to a magnetically ordered state and became either ferromagnetic, ferrimagnetic, antiferromagnetic or superparamagnetic. Meanwhile, above the transition temperature, thermal energy is sufficient to cause the moments to become disordered and loses its magnetization. For instance, the antiferromagnetic materials exhibit paramagnetic behavior above T_N.

A vibrating sample magnetometer or superconducting quantum interference device are powerful tools for the measurements of whole magnetization [32]. Fig. 4 shows the plots of magnetization against the magnetic field strength for paramagnetic, ferromagnetic and superparamagnetic [43]. Paramagnetic materials experience a net

increase in magnetic field as a result of an applied external magnetic field. Ferromagnetic materials displays a hysteresis loop as all domains do not return to their original orientations when decreasing the applied magnetic field after the saturation magnetization value is attained. Meanwhile, the thermal fluctuations in superparamagnetic particles are strong enough to spontaneously demagnetize a previously saturated assembly. Hence, these particles have zero coercivity and have no hysteresis loop on the magnetization curve.

Transmission electron microscopy (TEM) and scanning electron microscopy (SEM) are the main techniques applied to provide visual information on morphology such as size and shape of the prepared iron oxide. TEM is capable of generating images with higher resolution than SEM. X-ray diffraction (XRD) technique is commonly used to identify crystalline and composition of iron oxide. However, XRD analysis encountered a problem to distinguish between Fe_3O_4 and γ-Fe_2O_3 due to both systems possess an inverse spinel structure [24]. Thus, Mossbauer measurements in high external fields are needed to differentiate between Fe_3O_4 and γ-Fe_2O_3 through identification of the corresponding magnetic sub-lattices of the particles.

On the other hand, zero-field-cooled and field-cooled magnetization measurements are applied to estimate the blocking temperatures [24, 32]. This technique is related to the measurement of magnetization with increasing temperature in a weak applied magnetic field. Blocking temperature can be defined as the temperature between the blocked and the superparamagnetic state [43]. Superparamagnetic particles are usually ordered below a blocking temperature. Other physicochemical techniques such as Fourier transform infrared spectroscopy, thermogravimetric analysis, X-ray photoelectron spectroscopy and solid-state nuclear magnetic resonance have been used to investigate the surface properties of modified

iron oxide particles. Polshettiwar et al. [44] reported that Fourier transform infrared spectroscopy served as a better technique to characterize functionalized magnetic catalyst as compared to nuclear magnetic resonance. This is due to the magnetic nature of the material interferes with the magnetic field of the spectrometer. The above techniques provide important information for the magnetic properties and strength of bonding between the iron oxide surface and the coating.

2.3 Magnetic separation for water purification

Economic analysis is an important consideration for the selection of catalyst separation method in industrial treatment plant. Ambashta and Sillanpaa [34] reviewed the cost effectiveness of the separation technology based on the techniques such as reverse osmosis plant combined with magnetic separator and high gradient magnetic separation. Though the capital cost for the former technology is slightly higher than traditional reverse osmosis, the cost saving based on operation and maintenance improved the overall performance of the plant [45]. On the other hand, high gradient magnetic separation surpasses the conventional sand filter in terms of operating cost and sand requirement with the same installation cost for both technologies. Liu et al. [46] claimed that the pilot scale test (1000 m^3/d) for combining the magnetization with iron-based complex showed excellent performance for the advanced treatment of pulp and paper wastewater. The total operating costs including chemicals and power were about 0.13 US$/$m^3$, which could be accepted in industrial scale. Hence, water purification using magnetically assisted separation technology could be considered as an advantage with respect to time and cost saving.

The magnetic field used to separate the magnetic particles in the separation process can be generated by several ways [34]. The usage of permanent magnets normally creates a uniform magnetic field and electricity would not be utilized. Thus, it offers reduction in operating cost as the magnets are purchased only once at the early stage of installation and the strength of the magnet can last for many years [47]. The widely used electromagnets-based separator is high-gradient magnetic separator, which consist of solenoids of electrical conducting wires generating a magnetic field during electric current passage. When a magnetic field is applied across the wires, it generates large field gradients around the wires that attract magnetic particles toward the surfaces of wires. However, this magnetic field provided by electromagnets is limited only to separate particle sizes with several hundred microns [48]. Hence, superconducting magnet might be required to generate a stronger magnetic field to separate magnetic nanoparticles [48]. In short, three types of magnetic separators can be used for practical water purification in order to economically recover the magnetic nanoparticles from wastewater treatment.

3. Synthesis methods of iron oxide-based magnetic nanoparticles

In order to prepare homogeneous nanoparticles of iron oxide, a variety of synthesis routes such as co-precipitation reactions occurred in the mixture solution of Fe^{2+} and Fe^{3+} [14], thermal decomposition of organic iron precursor [16], solvothermal [18], hydrothermal [17] and microemulsion [19] method have been utilized. Magnetic particles obtained under different synthesis conditions may display differences in magnetic properties attributed to the changes in structural disorder, creation of anti-phase boundaries or the existence of a magnetically dead layer at the

particle surface [49]. The advantages and disadvantages of the various synthesis processes are briefly summarized in Table 1. These methods were found to be suitable to synthesis α-Fe_2O_3, γ-Fe_2O_3 and Fe_3O_4 with different proportions by controlling reaction conditions.

3.1 Co-precipitation

The most common method used to synthesize either Fe_3O_4 or γ-Fe_2O_3 is through co-precipitation of ferrous (Fe^{2+}) and ferric (Fe^{3+}) aqueous salt solutions by using an alkali such as sodium hydroxide (NaOH) or ammonium hydroxide (NH_4OH) [49]. The co-precipitation process involves the precipitation of iron precursors i.e. Fe^{2+} and Fe^{3+} at a molar ratio of 1: 2. The chemical co-precipitation can be expressed as Eq. (1) [38]:

$$Fe^{2+} + 2Fe^{3+} + 8OH^- \rightarrow Fe_3O_4 + 4H_2O \quad (1)$$

The size, shape and composition of the iron oxide nanoparticles depend on the type of salts used (e.g. chlorides, sulfates, nitrates), Fe^{2+}/Fe^{3+} ratio, reaction temperature, types of stabilizing agent, pH value, ionic strength of the reaction media and other reaction parameters [49, 55]. According to the thermodynamics of this reaction, a complete precipitation of Fe_3O_4 is expected to occur between pH 9 and 14, while maintaining a molar ratio of Fe^{3+}: Fe^{2+} as 2: 1 in an oxygen free environment. It should be highlighted that Fe_3O_4 is sensitive to oxygen and may undergo oxidation to $Fe(OH)_3$ or α-Fe_2O_3 phase in the presence of air as given in Eqs. (2) and (3) [49, 56].

$$4Fe_3O_4 + O_2 + 18H_2O \rightarrow 12\ Fe(OH)_3 \quad (2)$$

$$2Fe_3O_4 + \tfrac{1}{2}O_2 \rightarrow 3\alpha\text{-}Fe_2O_3 \quad (3)$$

Nitrogen gas was kept passing through the solution during co-precipitation to prevent oxidation of Fe^{2+} and reduces the particle size of Fe_3O_4 nanoparticles. Alibeigi et al. [14] and Mahmed et al. [57] found that reverse co-precipitation, in which a solution of Fe^{2+} added drop-wise into an alkaline solution in the presence of air can be used to produce Fe_3O_4 phase nanoparticles. They found that reverse co-precipitation of Fe^{2+}/Fe^{3+} mixed salt in alkali solution in an oxidizing environment would result in the formation of γ-Fe_2O_3 instead of Fe_3O_4 particles.

In short, co-precipitation method is simple and easy to obtain large quantities of magnetic particles. No special stabilizing agent is needed during the synthesis and the products are water-soluble which is promising for environmental-benign applications [15]. However, it is difficult to avoid the particles nucleation and subsequent growth during co-precipitation process. Consequently, the particles obtained through co-precipitation process are relatively large, broad size distribution, poor crystallinity, polydispersity, irregular in morphology and difficult to control their nanoparticle size and shape [58]. Hence, a size selection procedure after co-precipitation process will be needed in order to stabilize colloid solution or precipitate larger particles [24].

3.2 Thermal decomposition

Thermal decomposition of organometallic compound in high boiling organic solvent in the presence of various stabilizing surfactants has become a well-developed technique to achieve uniform and monodisperse iron oxide nanocrystals [16, 32]. The iron precursors can be either acetylacetonates [59], acetates [59], oleates [59], carbonyl [60], oxalates [59] or ferrocene [60], while benzyl ether or octadecene are used as high-boiling solvents [15]. The surfactants used include alcohol, oleic acid

and various types of organic amines i.e. oleylamine, trioctylamine, oleylamine, and hexadecylamine [16, 61]. In literature, primary amines and alcohols were used to accelerate the reaction rate and reduce reaction temperature [16]. Meanwhile, Wang et al. [16] studied the effect of various types of organic amines on the formation of iron oxide particles with spherical, truncated octahedral, cubic, and tetrahedral shapes. The obtained particle sizes typically vary between 5 to 30 nm depending on the synthesis condition.

Although the investigated iron sources were quite diverse, Yu et al. [62] believed that the precursors are transferred to iron carboxylate salts in the present of various surfactants. The carboxylate compounds were decomposed into iron oxide and several by-products such as carbon dioxide, carbon monoxide (CO), H_2 and hydrocarbons [16]. The decomposition reaction of metal carboxylates occurred at higher than 300 ^{o}C via the formation of thermal free radicals, which decreased the amount of iron complexes [63]. These radicals were able to recombine, decompose iron oleate complexes into smaller molecules or react with other metal carboxylate molecules to promote the overall reaction.

In contrast, Aniyaz et al. [59] demonstrated that the formation of an intermediate carboxylate complex produced by thermal decomposition of iron 2-methoxy-ethoxide in the presence of oleic acid showed a minor effect on the nucleation and growth of iron oxide nanocrystals. Singhal et al. [64] found that thermal decomposition of several iron complexes would form α-Fe_2O_3 at 750 ^{o}C and γ-Fe_2O_3 as intermediate products in regardless any ligand (mostly alkyl group) attached to iron. It is noteworthy that the reducing environment (CO) generated during thermal decomposition of the iron organic ligand complex led to the partial reduction of Fe^{3+} to Fe^{2+}, followed by the re-oxidation to FeO, Fe_3O_4 and α-Fe_2O_3 [65]. Hence,

iron organic species serves not only as iron precursor but also acted as a reducing agent of Fe^{3+} species.

Ellingham diagram is a well-known phase diagram to evaluate equilibrium phases between metal and metal oxides and can be used to determine the reduction feasibility of reducing any metallic oxide [66]. High oxidation temperature of iron leads to the formation of multilayer oxide scale according to the oxygen content of oxide, which are FeO, Fe_3O_4 and α-Fe_2O_3 [67]. Thus, Fe_3O_4 formation is a result from the local equilibrium between metallic iron and α-Fe_2O_3 [68]. The composition of the scale varies with oxygen partial pressure and temperature.

Nucleation occurred when the iron precursor was added into a heated solution in the presence of surfactant, while the growth stage took place at a higher reaction temperature. Wang et al. [16] reported that the nucleation temperature for the dissociation of iron oleate complex and growth of the magnetic nanoparticles occurred in a temperature range of 200–275 ^{o}C and around 300–330 ^{o}C, respectively. Size control and monodispersity can be achieved by the separation of the nucleation and growth steps, through control of the ramping temperature during synthesis [69]. Grzeta and coworkers [70] had demonstrated the relationship between the structure of α-Fe_2O_3 and γ-Fe_2O_3 together with the conditions of the thermal decomposition of iron-containing precursors. Fe_3O_4 or γ-Fe_2O_3 were obtained at 250–300 °C and α-Fe_2O_3 at 400–500 °C [65]. It was also found that prolonging the reaction time would favour grain growth. Besides, Snovski et al. [71] discovered that increasing duration time of the decomposition led to a decrement in the content of the iron oxide phases and an increment in the content of the iron carbide (Fe_3C). According to Zhou et al. [72], thermal decomposition of ferrous oxalate can provide various products by

controlling the reaction atmosphere. α-Fe_2O_3 could be obtained in air, γ-Fe_2O_3 in inert atmosphere or magnetite under limited air conditions.

In addition, more efforts need to be performed to investigate the complex mechanism of chemical conversions through thermal decomposition method into iron oxide due to the presence of multi-component reactants in the reaction mixtures. For instance, various type of components can be formed during the oxidative thermal decomposition of Fe(II) oxalate precursor including iron (α-Fe), FeO, α-Fe_2O_3 , γ-Fe_2O_3, Fe_3O_4, iron carbide (Fe_3C) and siderite ($FeCO_3$) [73]. Thus, more experiments investigating the role of variables such as reaction temperature, duration and initial hydrogen to carbon ratio should be conducted in controlling the types of organic compounds that are formed.

This organic thermal decomposition method has been proven to be a promising synthesis route for preparing high quality iron oxide i.e. Fe_3O_4 nanoparticles [74]. Fe_3O_4 nanoparticles produced via this method are monodisperse [58], high crystallinity [58] and can be tuned very well with respect to their size and shape [15]. However, thermal decomposition method suffers disadvantages such as requirement of relatively high reaction temperature [74], complicated procedures [74], usage of multiple reagents [74], possible emission of toxic gases like CO [16] and usage of expensive/toxic reagents which are not environmental friendly [58]. The particles obtained are usually insoluble in water or only soluble in certain non-polar solvents due to the non-polar characteristics of the initial oleate precursor ligand shell [15]. Thus, they need to be modified by additives such as polymers or long-chained water-soluble hydrocarbons to render them suitable for environmental applications. Therefore, future development on thermal decomposition method will shift towards

the preparation of water-soluble magnetic nanoparticles directly with less usage of multiple reagents.

3.3 Solvothermal and hydrothermal processes

A solvothermal process can be described as a reaction in the presence of any organic solvent such as methanol, ethanol or polyol in a closed system at a temperature higher than the boiling point of the solvent [74]. In an organic solvent-based synthetic route, the agglomeration of nanocrystals due to the anisotropic dipolar attraction can be avoided through the adsorption of surfactants onto the surfaces of nanocrystals [75]. Generally, the use of surfactant consists of a coordinating head group with significant affinity to various surfaces and a long alkyl chain for sterical hindering, which offers the base for the excellent stabilizing function of this ligand [76]. Several surfactants such as oleic acid [76] polyacrylic acid [77] and sodium dodecyl benzene sulfonic [77] have been used as capping agents during the solvothermal preparation of monodispersed iron oxide particles.

Polyol process refers to the usage of high-boiling polyols such as ethylene glycol, diethylene glycol, tri-ethylene glycol, tetra-ethylene glycol and propylene glycol to reduce metal salts to metal particles [77, 78]. The polyols could serve a triple role as high-boiling solvent, reducing agent and stabilizer to control the particles growth and prevent interparticle aggregation due to the steric interactions [78]. This can dispense the use of further surfactant in polyol process. The use of polyol in solvothermal process is the most simplest and efficient procedure in controlling the size and morphology of the iron oxide nanoparticles [77]. For instance, Kumar et al. [18] reported the synthesis of mono-dispersed 3D hierarchical microspheres

composed of nanospheres Fe_3O_4 using ferric chloride anhydrous acted as a precursor, while triethylene glycol acted as solvent and reducing agent. Besides, Xu and Zhu utilized a surfactant-free solvothermal route to fabricate hierarchiacally nanostructured hollow microspheres constructed by nanosheets in the mixed solvents of ethylene glycol and dimethylformamide [79]. They demonstrated that morphological control of iron oxide can be achieved by using different solvents.

The products obtained through this process are hydrophilic iron oxide nanoparticles which can be dispersed in aqueous solution and other polar solvents due to the coating of hydrophilic polyol ligands in situ [80]. In addition, high reaction temperature synthesis favors the formation of nanoparticles with high crystallinity, monodispersity and non-aggregated nanoparticles [80]. It has been reported that the size of iron oxide particles can be tuned by simply changing the concentration of precipitator NaOH and ratio of surfactant and precipitator [77].

In short, the advantages of this approach include no requirement for any reducing agent or surfactant except liquid polyols, kinetically control experimental conditions and easy scaling-up [78]. However, polyol process is very sensitive to the concentration of water and alkalinity [58]. Thus, it is still a challenge to control the size and surface properties of the iron oxide nanoparticles through varying the preparation reaction parameters.

On the other hand, hydrothermal process is a specific solvothermal process where water is employed as a dispersion medium instead of organic solvent [55]. High heat energy and pressure during hydrothermal treatment provide good revenue for the supercritical condition. The purpose is to enhance the dissolution of iron precursors as well as fracturing macronucleus particles to nanoscale particles [17]. However, several studies found that higher temperature could possibly result in bigger

particles size [55]. The resulting nanoparticles via hydrothermal process had weak agglomerated powders, narrow particle size distribution, low phase homogeneity as well as a high degree of crystallinity [17].

In the hydrothermal synthesis, organic compounds as well as polymers are usually used as dispersants and stabilizers. The organic dispersants include sodium dodecyl sulfate and polyacrylamide, while inorganic dispersants consist of sodium silicate, sodium phosphate and sodium stannate [81]. For example, α-Fe_2O_3 nanostructures have been synthesized hydrothermally using poly(vinylpyrrolidone) as surfactant and sodium acetate as precipitation agent [82]. Liang and co-workers [83] reported the synthesis of octahedral Fe_3O_4 crystals by hydrothermal treatment of potassium ferrocyanide with sodium thiosulfate additive. The advantages of hydrothermal synthesis include more cost-effective, high yield of products, excellent particles crystallinity with controllable size and good morphology of particles can be easily obtained [17].

Hydrothermal and solvothermal strategies are based on a general phase transfer and separation mechanism occurring between interfaces of solid and solution phases present during synthesis to produce a wide range of nanostructured materials [84]. The main disadvantage of hydrothermal and solvothermal methods is relatively slow kinetics due to the lower temperature used [85]. Microwave or ultrasound irradiations are more effective and attractive methods to synthesis nanocrystals with controllable size and morphology. Besides gaining more homogeneous heating process as compared with conventional heating, it can also promote nucleation, reduce the synthesis time and generate smaller particles [85]. Ultrasound-hydrothermal [86], microwave-hydrothermal [87], ultrasound-solvothermal [88] or microwave-solvothermal [85] routes were able to accelerate the kinetics of reaction. These

combination processes might lead to (a) rapid heating to the desired temperature; (b) increased reaction kinetics; (c) high phase purity; (d) high yield; (e) formation of novel phases; (f) selective crystallization and (g) good reliability and reproducibility [85, 87]. Thus, a rapid and facile approach to produce high quality of iron oxide nanoparticles is highly desirable.

3.4 Microemulsion process

Microemulsions are thermodynamically stable dispersions of immiscible water and oil phases, which stabilized by the arrangement of surfactant and co-surfactant molecules at the interface [89]. The microemulsion, especially water in oil emulsion or called inverse microemulsion consists of nanosized water droplets dispersed in an oil phase. It is stabilized by spherical reverse micelles which created by surfactant molecules at the water/oil interface [90]. These surfactant-covered water droplets can be considered as "nanoreactor" for the formation of nanoparticles. When two water nanodroplets collided, they will fuse and interchange reactants due to the driven force by Brownian motion [90]. This can inhibit excess aggregation of particles because the surfactants could adsorb on the particle surface when the particles approach to the water droplet [91]. Consequently, the particles obtained are generally very fine and monodispersed. Nanoparticles are formed when mixing two water-in-oil microelmulsions, where one containing a salt or a complex of metal (reactant 1), while the other contains a precipitating agent (reactant 2) as shown in Fig. 5 [92].

Since the chemical reaction is limited to the nuclear interior of water molecules [90], it is possible to manipulate the particles size, shape and regulate narrower particle size distribution by controlling the amount of the mixture oil/water/surfactant

[89]. Various morphologies can be obtained by proper control of the preparation conditions. Zhang et al. [91] had reported on the synthesis of hollow Fe_3O_4 submicrometer-sized spheres in a microemulsion system using sodium dodecyl benzene sulfonate as surfactant. Besides, well-defined grass-like [19] and flower-like Fe_3O_4 [93] structures had been successfully synthesized via a microemulsion-assisted solvothermal method.

Microemulsions provide advantages such as economical, environmental friendly synthesis process and uniform nanoparticles without going through any size-selection process [94]. However, the major drawbacks of this process are the usage of large amount of solvent to synthesize appreciable amount of nanomaterials and the adverse effects of residual surfactants on the properties of the particles [32]. Thereby, the indication of scale-up production depends relatively on the amount of nanoparticles that could be produced in a single reaction.

4. Photocatalysts and photocatalytic reactions

The photocatalytic degradation reaction receives great interest in the field of wastewater treatment due to its complete mineralization with mild operating temperature and pressure. Photocatalytic reactions proceed when organic molecules are in direct contact with the catalyst surface. The photocatalytic activity of photocatalyst towards a specific reaction depends on its physicochemical properties, optical property and external conditions [95]. The physicochemical properties include the morphology, particle size, degree of aggregation, surface area and crystallinity of photocatalyst. The optical absorption property is related to electronic band gap structure, while external conditions are related to the operating conditions of

photocatalytic reactions. To date, most of the reviews have been focusing on the heterogeneous photocatalysis and it is very rare to find review works dedicated to magnetic type photocatalysts.

4.1 Principles of photocatalyst

Fig. 6 shows the schematic diagram of relative band positions with respect to the absolute vacuum energy scale (AVS) and normal hydrogen electrode (NHE) at pH = 0 for various types of semiconductors [3, 96]. It also gives the redox potentials of the H_2O/O_2, hydrogen ion (H^+)/hydrogen (H_2) and O_2/superoxide anion radical ($\bullet O_2^-$) couples which are applicable for water splitting. The relative position of the band edges as compared to redox potentials of species and band gap energy of the material are important to determine the field of application. For example, in order to perform photolysis of water by illumination of light, the conduction band should lay higher than that of the species to be reduced and the valence band should locate lower than that of the species to be oxidized [3].

4.2 Example of existing photocatalysts

In the past few years, numerous active photocatalysts had been extensively investigated. TiO_2 is the leading candidate among various semiconductor-based photocatalysts due to its high photo-activity, high chemical and thermal stability, low toxicity and relatively lower cost [97]. TiO_2 fulfils the basic requirement of photocatalysis as compared to other metal oxides as shown in Fig. 6. The generated holes have sufficient energy to oxidize a wide range of compounds, while electrons

are able to reduce O_2 molecules. TiO_2 exists in three main crystallographic forms: anatase, rutile and brookite. The band gap energies for anatase, rutile and brookite are about 3.2 eV, 3.0 eV and 3.2 eV, respectively [97]. Their different lattice structures and electronic band structures resulted in the disparity in their photocatalytic properties and anatase often showed a higher photocatalytic activity in most cases. ZnO with a band gap energy of 3.2 eV, is also an excellent photocatalyst owing to its high photocatalytic activity, environmentally friendly nature and relatively low cost [1]. The photocatalytic activity is expected to be similar to that of TiO_2 due to the similar energy level of conduction and valence bands (Fig. 6). The main drawback is related to its unsatisfactory photostability in wide pH range of solution.

Tin dioxide (SnO_2) is a wide band gap energy semiconductor (3.6–3.8 eV) and requires UV light with a wavelength shorter than 330 nm for its photonic excitation [98]. The photo-generated hole in the valence band of SnO_2 is more anodic and has higher oxidizing power than TiO_2 and ZnO, while the conduction band electron in photo-excited SnO_2 is less cathodic than that of iron oxide [99]. SnO_2 alone is rarely used as photocatalyst due to its position of conduction band, which is incapable to reduce oxygen molecules as shown in Fig. 6. However, it may serve as a potential photocatalyst when coupled with other semiconductors with proper matching of band levels.

Common photocatalysts usually encountered narrow light response range due to wide band gap energy and low quantum efficiency because of high recombination probability of the photogenerated electron-hole pairs. This resulted in the restriction for applications of these photocatalyts. Hence, semiconductors with small band gap energies like metal sulfide have been proven to be one of the most attractive visible light-driven photocatalysts. In particular, cadmium sulfide (CdS) with relatively

narrow band gap energy of 2.3–2.4 eV has been intensely studied due to its ability to harvest visible light [100, 101]. However, it is susceptible to photo-corrosion by photo-generated holes in aqueous media due to its low conduction band edge. In addition, bismuth-containing semiconductor photocatalysts appear to be good candidates as photocatalysts. The reasons are due to their non-toxicity, chemically and thermally stable and most of them have strong response to visible light owing to the interactions between Bi (6s) and O (2p) orbitals above the valence band [102].

Tungsten oxide (WO_3) has been extensively studied due to its long term stability during irradiation, resilience to photo-corrosion effects and strong absorption of light in the UV-visible region [103]. WO_3 with band gap energy about 2.6–2.8 eV possesses strong oxidation power for photo-generated holes [103, 104]. These characteristics render it as an attractive candidate for visible light responsive photocatalyst for photocatalytic degradation of organic pollutants. Although its valence band position reveals its capability to oxidize various organic compounds, WO_3 does not has the ability to reduce H^+ to H_2 unlike other chalcogenide semiconductors.

Besides, iron oxide possesses strong oxidation power due to its valence band edge exceeding the standard redox potential of H_2O/O_2. The drawbacks of iron oxide include the energy of conduction band of iron oxide relative to the H^+/H_2 couple is low to drive the hydrogen evolution reaction, unfavorable conduction band electrons transfer to dissolve O_2 and its short hole diffusion length for surface reactions [105]. However, iron oxide with the advantages of ease in preparation at high purity, absorption at longer wavelengths and its higher stability during irradiation are very attractive for photocatalytic research.

In addition, various types of carbonaceous materials such as carbon nanotubes [106], conjugated carbon materials like graphene [107] and graphene oxide [108] have received a lot of attention in the application of photocatalysis. This is due to their high surface area [108], optically transparent [108], high adsorption, mechanical and thermal properties [109], chemical inertness and stability [109]. For instance, carbon nanotubes have unique hollow, layered structure and large electron-storage capacity, which may accept photon-excited electrons and leads to a fast electron transport along the cylindrical nanostructure [109]. Thereby, this retarded the recombination rate of the photo-generated electron-hole pairs. On the other hand, conjugated carbon materials with π structures are able to delocalize the photo-generated electrons through its π network [108]. This induces a rapid charge separation and inhibites charge recombination in electron-transfer processes.

Until now, majority research works are performed using nanoparticle photocatalysts suspended in the wastewater. The main advantages of this slurry system are (1) better availability of the catalytic surface area for adsorption and reaction (2) good mass transfer of the wastewater contaminants to the photocatalyst. The major problem which hinders their wide scale application in industry is the need to separate them for recycles during post treatment. It is uneconomical and troublesome to separate nano- or micro-sized particles from large volume of water via sedimentation or filtration. As a consequent, system using immobilization of photocatalyst related research has been reported. Its process efficiency will be reduced when the catalyst is stationary even though with the same catalyst loading, most probably due to lower ratio of catalytic surface area per volume of the treated liquid and limited mass transfer [110]. In conjunction, magnetic type of photocatalysts

present several advantages such as easy to be recycled and suspended in the water medium to increase the contact possibility of pollutants with photocatalysts.

4.3 Mechanism of photocatalytic reaction

Photocatalytic process occurs based on the sufficient energy obtained from the absorption of light radiation which equals to or is greater than the semiconductor band gap energy. Fig. 7 shows the photocatalytic reactions proceed on a semiconductor material. When the energy of incident light is larger than the band gap of a semiconductor material, electrons in valence band will be excited to the conduction band and leaving holes in the valence band. The excitation creates electrons (e^-_{cb}) in conduction band and holes (h^+_{vb}) in valence band in fs time scale (Eq. (4)), which are subsequently trapped in 100 ps (shallow trap) to 10 ns (deep trap) and recombine with each other in the range of 10–100 ns (Eq. (5)) [111]. The photo-induced electrons participate in the reduction processes, in which they will react with the adsorbed oxygen or oxygen dissolved in water to produce $\bullet O_2^-$ (Eq. (6)). $\bullet O_2^-$ may then react with H^+ to generate hydroperoxyl radical (•OOH) (Eq. (7)) and proceed further to form hydrogen peroxide (H_2O_2) (Eqs. (8) and (9)) [111]. The electrons could react with H_2O_2 and reduce it to •OH (Eq. (10)). Meanwhile, the photo-induced holes diffuse to the TiO_2 surface, react with the adsorbed water molecules in neutral solution (Eq. (11)) or the adsorbed hydroxyl group in alkaline solution (Eq. (12)) to form •OH [111]. •OH can degrade most of organic compounds with second-order rate constants of 10^8–10^{10} M^{-1} s^{-1} [112]. The reactive oxygen species and holes may contribute to the oxidative pathways such as the degradation of a pollutant as shown in Eqs. (13)–(16) [97].

$$\text{Semiconductor} + \text{Energy (heat or light)} \rightarrow h^+_{vb} + e^-_{cb} \quad (4)$$

$$h^+_{vb} + e^-_{cb} \rightarrow \text{Energy (heat or light)} \quad (5)$$

$$O_{2(ads)} + e^-_{cb} \rightarrow \bullet O^-_2 \quad (6)$$

$$\bullet O^-_2 + H^+ \rightarrow \bullet OOH \quad (7)$$

$$\bullet OOH + e^-_{cb} \rightarrow \bullet OOH^- \quad (8)$$

$$\bullet OOH^- + H^+ \rightarrow H_2O_2 \quad (9)$$

$$H_2O_2 + e^-_{cb} \rightarrow \bullet OH + OH^- \quad (10)$$

$$H_2O_{(ads)} + h^+_{vb} \rightarrow \bullet OH + H^+ \quad (11)$$

$$OH^-_{(ads)} + h^+_{vb} \rightarrow \bullet OH \quad (12)$$

$$\text{Pollutant}_{(ads)} + h^+_{vb} \rightarrow \bullet\text{Pollutant}^+ \rightarrow \text{degradation products} \quad (13)$$

$$\text{Pollutant} + \bullet O^-_2 \rightarrow \text{degradation products} \quad (14)$$

$$\text{Pollutant} + \bullet OOH \rightarrow \text{degradation products} \quad (15)$$

$$\text{Pollutant} + \bullet OH \rightarrow \text{degradation products} \quad (16)$$

where subscripts 'ads' denote the adsorbed form of the molecule.

After water treatment, the separation of nanocatalyst from treated water remains problematic due to the difficulty, time-consuming and cost-expensive separation process, especially when dealing with large volume of treated water [113]. Hence, magnetic nanoparticles have been receiving great attention and widely utilized in environmental purification.

4.4 Iron oxide as magnetic photocatalyst

The magnetic properties i.e. magnetic moment of iron oxide is mainly due to the uncompensated electron spin of the individual ions and the spin alignments in the two sublattices [114]. It has been reported that the spin degeneracy of the bands in the magnetic semiconductor is lifted and the unwanted recombinations are impeded by spin selection rules or by low occupancy of states involved in the allowed recombinations [115]. In turn, it could enhance the photoenergy conversion efficiency due to the improved visible-light absorption, charge separation, mobility and lifetime. Besides, the behavior of electrons, holes and free radicals might be influenced by the Lorentz force in the magnetic field, which stemming from the remanent magnetization of magnetic catalyst during photocatalysis [116, 117].

The application of external magnetic field has an effect on the free radical reactions and recombination rate of the photo-generated electrons and holes, which subsequently affecting the catalytic activity [118]. Meanwhile, research work focused on the correlation between magnetic properties of catalyst and photocatalytic activity is still quite limited [119]. Nevertheless, there is an intimate relationship between the magnetic properties of atoms in the active sites of the catalyst and its catalytic activity. The catalytic activity is due to the chemical valence forces of the atoms on the catalyst surface while the free valence of atoms is based on the orbital magnetic moments and spin [120]. Therefore, the catalytic activity of catalyst depends on the nature of atoms active centers.

Apart from the light excitation of iron oxide to separate electron-hole pairs and produces reactive oxygen species as shown in Eqs. (4)–(12), the radicals generation by Fe^{2+} and Fe^{3+} ions on iron oxide surface should also be considered. During photocatalytic process, traces of iron ions might penetrate the coating of passive layer [121]. The presence of iron ions in aqueous solution can accelerate the organic

pollutant degradation by Fenton (Fe^{2+}/H_2O_2) and Fenton-like (Fe^{3+}/H_2O_2) reactions mechanism. In Fenton process, Fe^{2+} is oxidized to Fe^{3+} to generate •OH (Eq. (17)). Then, Fe^{2+} is regenerated through the reduction of Fe^{3+} by H_2O_2 (Eq. (18)).

$$Fe^{2+} + H_2O_2 \rightarrow Fe^{3+} + \bullet OH + OH^- \quad (17)$$

$$Fe^{3+} + H_2O_2 \rightarrow Fe^{2+} + \bullet O_2H + H^+ \quad (18)$$

The Fe^{2+} on iron oxide surface can further react with the oxygen dissolved in the reaction mixture to generate Fe^{3+} ions and reactive oxygen species including $\bullet O_2^-$, H_2O_2 and •OH as shown in the reactions (19)–(23) [1, 122, 123]. These radicals serve important implications for the photocatalytic degradation of organic pollutants. Fang et al. [122] had proposed a mechanism pathway for the generation of these active radicals by magnetic iron oxide. A modification has been made to describe completely the degradation mechanism of organic pollutants by iron oxide as shown in Fig. 8.

$$Fe^{2+} + O_2 \rightarrow \bullet O_2^- + Fe^{3+} \quad (19)$$

$$Fe^{2+} + \bullet O_2^- + 2H^+ \rightarrow Fe^{3+} + H_2O_2 \quad (20)$$

$$\bullet O_2^- + H^+ \leftrightarrow \bullet O_2H \quad (21)$$

$$2\bullet O_2^- + 2H^+ \rightarrow H_2O_2 + O_2 \quad (22)$$

$$\bullet O_2^- + H_2O_2 + H^+ \rightarrow O_2 + \bullet OH + H_2O \quad (23)$$

5. Fabrication of iron oxide photocatalysts

It should be noted that different synthesis processes will produce different morphologies of iron oxide particles as shown in Fig. 9 [24]. Besides bare iron oxide (Fig. 9 (a)) [74], the most widely investigated structure is core-shell type (Fig. 9 (b)) [124], in which the iron oxide phase is the core and another semiconductor phase

acted as the shell. Other structures include multinuclei-type (Fig. 9 (c)) [125], bead-on-bead type where magnetic nanoparticles are deposited on semiconductor (Fig. 9 (d)) [126] and metal nanoparticles are deposited in mesoporous magnetic material (Fig. 9 (e)) [127]. The information compiled in Table 2 were evaluated and discussed by considering different types of iron oxide photocatalyst as the major parameter.

5.1 Iron oxide

Three forms of iron oxide materials i.e. α-Fe_2O_3, γ-Fe_2O_3 and Fe_3O_4 can be considered as good photocatalysts due to the appropriate valence band position for oxygen evolution and narrow band gap energies [4, 5]. These factors favor the generation of electron-hole pairs and participate in the reduction and oxidation processes. Iron oxide materials suffered short hole diffusion length (2–4 nm) and poor electron mobility in the range of 0.01 cm^2/Vs^4 to 0.1 cm^2/Vs^4 [2], which resulted in rapid recombination rate of electron-hole within nanosecond [141]. These drawbacks of iron oxide materials are the major challenges for their practical application. Among different types of iron oxide, α-Fe_2O_3 is the most stable iron oxide under ambient conditions [142]. Although Fe_3O_4 has higher saturation magnetization than γ-Fe_2O_3, γ-Fe_2O_3 possesses better chemical stability due to the fact that Fe_3O_4 nanoparticles can dissolve in acidic medium [143]. Thus, Fe_3O_4 can be deliberately oxidized to γ-Fe_2O_3 in order to avoid this dissolution.

It is well understood that photocatalytic properties are largely depended on the morphology, particle size and specific surface area [144]. Recently, nanostructuring techniques have been proven useful in increasing the catalytic performance of iron oxide due to excellent chemical and electronic properties of various morphologies.

The conduction and valence band edge relative to the redox potential of the adsorbates play important roles in the charge transfer processes [145]. The higher the conduction band edge, the larger the reductive power of the electrons. Iron oxide can be synthesized in various morphologies such as zero-dimensional (0D) nanocrystals (particles, cubes) [16, 144], one-dimensional (1D) nanocrystals (rods, wires, tubes, and belts) [2, 128], two-dimensional (2D) nanocrystals (disks, platelets, sheets and films) [79], three-dimensional (3D) nanocrystals (dendrites, flowers, sea-urchin-like and spheres) [18, 144].

0D nanosphere semiconductors as photocatalysts often encountered strong quantum confinement effect, which resulted in high recombination rate of photo-generated electrons and holes [23]. 1D nanostructures with increasing ratio of length to diameter could restrict electrons flow in radial direction and instead guide the movement of electrons through axial direction. It had been reported that aligned α-Fe_2O_3 nanotubes were able to achieve enhancement of surface area without an increase of the geometric area and reduce the scattering of free electrons, thereby, enhance the electrons mobility [2]. Besides, hollow structures i.e. α-Fe_2O_3 nanorings exhibit high light harvesting, absorption efficiency and a fast motion of charge carriers [128]. Meanwhile, 2D structures can provide a lot of reactive sites on the surface and exhibit intriguing charge bearing properties owing to its large surface area [23]. The 3D structures i.e. micropine dendritic iron oxide photocatalysts with its large surface area and special pore channels allow high mass transfer rate of the reactants and products [23, 144]. All these nanostructures materials are expected to achieve higher photocatalytic activities. For instance, Sutka et al. [146] demonstrated that 2D Fe_3O_4 nanoparticles (nanoflakes) exhibited higher saturation magnetization *and* coercive force attributed to their greater surface area and smaller particles. They

reported that 2D structures could also be used as carriers for other photocatalysts such as TiO_2 which were magnetically recyclable.

Iron oxides are solar energy conversion materials and have been found to be highly active catalysts for the photocatalytic degradation of organic pollutants. However, high recombination rate of charge in iron oxide lowered its degradation efficiency and limits its photocatalytic performance. Hence, several recommendations have been taken to improve its efficiency such as heteroatom doping, noble metal loading and composites with other semiconductors.

5.2 Doped iron oxide

Iron oxide commonly exhibits low photocatalytic ability due to slow charge transfer, short hole diffusion length and high recombination rate of electron-hole [128]. Thus, modification of iron oxide is a useful strategy for the improvement of electron-hole separation and catalysis enhancement. Beside fabricate different nanostructures with well-defined shapes, an alternative modification strategy is the incorporation of heteroatoms into iron oxide materials. Even though conduction band level of α-Fe_2O_3 is not negatively enough to reduce water to hydrogen ion directly, the incorporation of transition metals could modify the conduction band edges of iron oxide cathodically [147].

Various types of dopant species such as Pt [148], molybdenum (Mo) [149], chromium (Cr) [149], Ga [130], Ba–Cd–Sr–Ti [131] and S [142], had been introduced into iron oxide in order to improve its photocatalytic activity. For instance, Tang et al. [147] found that charge-compensated donor-acceptor i.e. Ti–Mg co-alloying photocatalyst could minimize the drawbacks encountered by Ti–Fe_2O_3. Ti–Mg co-

alloyed iron oxide could enhance the solubility of Mg and Ti, which led to the reduction of electron effective mass and therefore increased electron mobility. Besides, it could reduce the density of charged defects and thereby reduce charge carrier recombination. Consequently, Ti and Mg co-alloyed α-Fe_2O_3 exhibited improved water oxidation as compared to pure α-Fe_2O_3. Note that the dopant ions should be prepared within an appropriate concentration so that the dopants can selectively trap one charge carrier and allow another one to reach the particle surface for the subsequent redox reactions [130]. Beyond the optimum concentration, dopant ions could act as recombination centers for the photo-generated electrons and holes which will subsequently decrease the photocatalytic performance. More examples of doped iron oxide and its functionalities in photocatalytic degradation performance are presented in Table 2.

5.3 Metal-loaded iron oxide

One of the potential strategies is to modify iron oxide with co-catalysts, usually loading with noble metal nanoparticles such as Pt [134] and palladium (Pd) [150], silver (Ag) [151] and Au [133]. Noble metal nanoparticles are known to have unique electronic and catalytic properties, which are able to enhance the photocatalytic activities of the semiconducting materials [128]. It had been reported that Schottky barrier would form at the metal-metal oxide interface [133]. In such structures, metal oxide usually serves as the light harvesting component to absorb photon and separate electron-hole pairs. The separated electrons can readily move through the hetero-interface, while holes will localize in the lower energetically metal oxide due to the contact between metal oxide and metal nanoparticles with higher electronegativity.

For example, Liang et al. [128] reported that the effective electron-hole separation in the hybrid α-Fe_2O_3/Pt nanorings resulted in significant improvement of the photocatalytic performance. As shown in Fig. 10, Pt served as the conduction band electron sink owing to its lower Fermi level. The photo-induced electrons transferred from α-Fe_2O_3 to metal particles would be trapped by dissolved oxygen molecule, while holes left on the surface of α-Fe_2O_3 nanorings would then reacted with hydroxyl groups. This promotes the interfacial charge separation at the metal-α-Fe_2O_3 interface.

In addition, noble metal nanoparticles exhibit strong visible light absorption due to their localized surface plasmon resonance [133]. Such noble-metal particles have the property of collective free electron charge when excited by visible light. The plasmon-induced electrons are transported from photo-excited noble-metal particles to the conduction band of the semiconductor. This facilitated the separation of electron-hole pairs [152].

Although noble metals can significantly accelerate the photocatalytic reaction rate, the high cost of noble metals greatly limits their practical applications in large scale. It should be noted that majority of the research works showed that only a minor amount of noble metal was required to load on the photocatalyst to improve its photocatalytic activity. Hence, the optimization amount of loading is important as high amount of noble metal could minimize the absorption of incident light by the metal nanoparticles. They could also serve as recombination centers for photo-generated electrons and holes [151].

5.4 Composite semiconductors

Coupling of iron oxide with either oxide or other non-oxide photocatalysts (so-called composite photocatalyst) is another approach to increase the photocatalytic activity through efficient charge separation and enhanced visible light absorption. Composite or nanocomposite materials [153] provide the possibility for enhanced functionality and multifunctional properties in contrast to their more-limited single-component counterparts. Recently, core-shell type is one of the composite examples widely investigated [104, 135]. The iron oxide magnetic core is beneficial for recovery of suspended particles from the treated solution, whereas the outer shell can be used as photocatalyst to destroy organic pollutant in wastewater [154]. Thus, it is important to choose suitable shell material with compatible physical and chemical properties compare to core material.

The relative positions of the conduction and the valence bands of various semiconductors are shown in Table 3. Based on the energy level of both types of semiconductors, Fig. 11 shows the thermodynamically feasible pathways for the charge carriers in the form of core-shell structured as well as bead-on-bead type structured composites [155]. When dual semiconductors with different energy levels were contacted, the photo-generated electron could be transferred to the lower level conduction band of the semiconductor [155]. Meanwhile, the photo-generated holes might also be transferred to the upper level valence band of the semiconductor. In Fe_2O_3–TiO_2 heterojunction, the photo-generated electrons in the valence band of TiO_2 can be injected into Fe_2O_3, while photo-generated holes accumulated in the valence band of TiO_2. This interfacial charge transfer between the two semiconductors would facilitate the charge separation, which resulted in a delay in the electron-hole recombination and accelerates the oxidation efficiency by holes and reduction rate by electrons.

Similarly, when a large band gap semiconductor was coupled with a small band gap semiconductor with a more negative conduction band potential energy level, photo-generated electrons could be injected from the small band gap semiconductor into the large band gap semiconductor. The examples of this type of heterostructures include the composite of WO_3/α-Fe_2O_3 [103] and SnO_2/α-Fe_2O_3 [98]. Both of these research works demonstrated that smaller band gap energy of α-Fe_2O_3 was suitable for capturing visible spectrum light to excite electrons from valence band to its conduction band [103]. Then, the photo-generated electrons will be transferred from conduction band of α-Fe_2O_3 to the conduction band of another semiconductor since conduction band of α-Fe_2O_3 is more cathodic than WO_3 and SnO_2. This led to the separation of the electrons and holes across the heterojunction. In short, Fe_2O_3 could act as a sink for photo-generated electrons [157] or a source for photo-generated electrons [103] depending on the potential energy position for both of the heterostructures.

Qin et al. [158] and Akhavan and Azimirad [159] also claimed that narrow band gap energy of Fe_2O_3 could be utilized as a sensitizer to absorb more light and excite more electron-hole pairs for larger band gap energy of semiconductor. Charge separation and transport improvements are two important ways to improve catalytic efficiency. Excited electron-hole pairs which are not separated and transport to anode or cathode in time will result in subsequent charge recombination to occur. Beydoun and co-workers [155] believed that the incidence of electron-hole recombination rate increased in narrower band gap energies of iron oxide phases, especially in the case of Fe_3O_4 with the continuous hopping between Fe^{3+} and Fe^{2+} in the lattice [154]. In other words, the proportions of these separation-interface transport and recombination effects could decide the net contribution to the catalytic activity. Thus, the key

challenge is to find an efficient inorganic semiconductor with appropriate electronic states to enhance the charge separation and fast transfer of photo-generated electrons and holes from one semiconductor to another.

However, coupling of semiconductors does not always enhance charge separation as the design relies on the electronic band structures of its components, which are in turn determined by various factors such as surface area, crystallinity, defect and quantum size effects. Several researchers had reported that certain electronic heterojunction between semiconductor and iron oxide composites will lead to the unfavorable electron-hole recombination and thereby lowered oxidizing power of the photo-generated holes [155]. Consequently, composite semiconductor and iron oxide photocatalysts suffered dramatical decrement in photocatalytic activities.

For instance, the semiconductor i.e. TiO_2 coated on the iron oxide phase was usually in amorphous phase and it required high temperature calcination to obtain its crystalline product [160]. However, heat treatment process resulted in the loss of surface area due to the sintering and crystal growth of the resultant products. It also caused the loss of magnetism properties due to the porosity of the semiconductor coating, partial oxidation of the iron oxide core or the formation of a mixed iron and titanium oxides [161]. Hence, surface coating and surface modification were investigated in order to prevent interactions between the iron oxide-based magnetic core and the semiconductor coating.

5.5 Encapsulation of iron oxides

Iron oxide-based magnetic particles tend to agglomerate and form large clusters due to the magnetic dipolar attraction, resulting in loss of specific surface area and

active sites [49]. Besides, iron oxide-based magnetic particles are easily oxidized by air and thus destroy their high magnetic moment [162]. Therefore, the issue of maintaining the stability of iron oxide-based magnetic particles such as preventing aggregation or precipitation and protect from air oxidation are desirable. Intensive efforts have been made on the encapsulation of magnetic nanoparticles.

The applied coating can be organic (i.e. surfactants equip with functional reactive group like hydroxyl, aldehyde, amino and carboxyl group), inorganic components (i.e. SiO_2, carbon) and organic/inorganic polymer. The organic coating can prevent agglomeration of particles [51], while the inorganic coating can enhance thermal stability, acid resistance of core in corrosive solution, used for functionalization and protect iron oxide from photo-dissolution and oxidation [163]. Ferroudj et al. [164] claimed that reactants were able to diffuse through micropores inside SiO_2 matrix and in contact with active sites of iron oxide nanoparticles. This kind of magnetic species is intrinsically active for catalytic reaction as well as separation. Since the effect of shading due to coating material is unavoidable, the catalytically active sites which bounded on the outer surface of the support to avoid the pore diffusion constraint can help to overcome this disadvantage.

For inorganic matrix, SiO_2 has been widely used as coating on iron oxide-based magnetic nanoparticles due to its low cost material [8], high stability against chemical degradation [126], under aqueous solution especially low pH solution [32] and widely available with relatively large surface area [8]. Deng et al. [165] had described several advantages for SiO_2-coated iron oxide-based magnetic nanoparticles. SiO_2 coating could screen the magnetic dipolar attraction between magnetic nanoparticles, which then favored the dispersion of magnetic nanoparticles and protected the leaching phenomenon. SiO_2-coated iron oxide-based magnetic nanoparticles could be easily

activated or surface modified due to the existence of abundant silanol groups on the SiO_2 layer that are compatible with various functional groups such as amines, thiols and carboxyl group [57]. SiO_2 layer also provides a chemically inert surface which is beneficial for various catalyst modifications and applications. However, it was found that the ideal spherical shapes of SiO_2-coated iron oxide-based particles are difficult to be produced in large scale due to the strict reaction condition [166]. Besides, SiO_2 is unstable under basic condition and there is a possibility that oxygen or other species diffuse through the porous SiO_2 materials [32].

In order to avoid low photocatalytic activity created by magnetic core-semiconductor shell i.e. Fe_3O_4-TiO_2 as reported by Beydoun et al. [155], SiO_2 layer was proposed to coat on the iron oxide-based magnetic particles before subsequent coating with TiO_2 particle. This could inhibit the photo-generated electrons and holes in the TiO_2 particles transferred to the magnetic core particle rather than to the TiO_2 surface. It was believed that SiO_2 layer could prevent iron oxide-based magnetic particles from acting as an electron-hole recombination center [154]. On the other hand, Kishore and Jeevanandam [126] reported that SiO_2 microspheres can also be used as core, while iron oxide nanoparticles as shell for the applications in catalysis and environmental remediation.

As compared to the generally used SiO_2 material, carbon-based material is another special and unique material for coating purpose. The advantages of carbon-based materials include high chemical and thermal stability, possible to have various pores, low toxicity, radiation resistant and high biocompatibility [167]. Liu et al. [168] reported that amorphous carbon can be obtained via inexpensive and environmental friendly process by using glucose as a precursor. They found that the distributed nano-sized pores on the surface of carbon coating could increase the surface area and

facilitated penetration of reactive species. Additional functionalities might be introduced into the carbon coatings, subsequently alter the optical properties, catalytic or absorbing capacity [168].

The abundant amount of –OH and $–COO^-$ groups on the surface of amorphous carbon could bind with metal cations through coordination or electrostatic interactions. As a result, these functional groups on the carbon layer could give rise to the preferred sites of nucleation. Therefore, absorption of metal ions such as Au, Ag, and Pt nanocrystals followed by the growth of the crystals on the surface of reactive carbon layer are relatively easier [140]. However, carbon-based coating materials often encountered disadvantages such as agglomerated clusters due to the lack of effective synthesis methods and poor understanding on the formation mechanism [32].

The investigated polymer materials coating include poly amidoamine dendrimers [138], poly(ethyl methacrylate-co-methacrylic acid) [22], poly(acrylic acid) [106], polystyrene [166], poly(vinyl alcohol) [166], polyethylene glycol [169] and poly(vinylpyrrolidone) [170, 171]. The iron oxide-based magnetic particles can be covered by polymeric particles through either physical interactions or chemical reactions [22]. The functional groups of polymers such as carboxylic acids, phosphates and sulfates can be grafted on the surface of inorganic materials by stable covalent bonding. Polymers coated iron oxide resulted in materials of high mechanical strength, high thermal stability and superior optical, magnetic and electric properties [22]. Besides, polymer at the surface presents high selectivity, binding kinetics, more accessible sites and high mass transfer rate [172].

For example, magnetic polystyrene particles possess excellent size distribution and spherical shapes with hydrophobic surface [166]. Chen et al. [106] investigated the photocatalytic activity of Pt-doped TiO_2-coated iron oxide-based magnetic coated

by polymeric microspheres on the degradation of dimethyl phthalate. They demonstrated good repeatability of the photocatalytic performance with the use of the resultant photocatalyst in the multi-run experiments. Meanwhile, Kim et al. [138] found that the enhancement of photocatalytic activity using iron oxide-based magnetic-cored dendrimers with nano-sized TiO_2 was attributed to the electron captured in dendrimers, which restrained recombination rate of electron-hole pairs.

However, the preparation of polymer coated on reactive iron oxide-based magnetic nanoparticles would encounter drawbacks such as unstable in air atmosphere, at higher temperature and easily leached in acidic solution [32]. It should be bear in mind that the encapsulation of inorganic nanoparticles in a polymer matrix leads to phase separation due to the incompatibility between organic and inorganic materials [22]. Thus, the surface modification via hydrogen bonding, electrostatic interactions or covalent bonds within the inorganic/organic interface need to be investigated in order to enhance the compatibility between the two materials.

From the viewpoint of practical application, it remains a major challenge to solve the poor stability and a sudden drop in catalytic activity of the encapsulated magnetic particles. Encapsulated protective layer had indicated potential improvement for the stability of magnetic particles in suspension. Yet, the challenge of without sacrificing the catalytic activity should be taking into account. A promising synthesis method to fabricate a magnetic particle containing capsulate with a thin and permeable coating to obtain enhanced stability at an insignificant decrement in catalytic activity should be focussed. Wang et al. [173] suggested that magnetic Fe^0/Fe_3C particles could be encapsulated by porous carbon sphere for enhancement of transportation and suspension without significantly reducing its catalytic activity.

Hence, the best compromise between catalytic activity and stability will be the most preferable to be used in broad application as catalysts.

6. Toxicity effect and future perspectives

It is noteworthy that materials in nanoscale range present an important emerging class of contaminants which have wide ecological impacts within marine and estuarine ecosystems [174]. It is imperative to identify the ecotoxicity of iron oxide-based magnetic nanoparticles in aquatic environment due to the possibility of direct exposure to humans via skin contact, inhalation and direct ingestion of contaminated drinking water [141]. Several groups of researchers had studied the toxicity effects on the use of iron oxide nanoparticles. Liu et al. [175] evaluated single and repeated dose toxicity of superparamagnetic iron oxide nanoparticles by giving injection to mice. Their results confirmed that iron oxide nanoparticles had low hazard potential to mice and histopathological evaluation revealed no iron positive pigments in macrophages from major organs like liver, lungs, spleen, brain, kidney and heart.

However, a few reports had suggested some toxicological effects for superparamagnetic iron oxide nanoparticles. For example, Mahmoudi et al. [176] found that polyvinyl alcohol coated iron oxide nanoparticles induced less cytotoxicity due to fewer adsorption sites available for interaction with proteins and other biomolecules in mouse connective tissue cells L929 as compared to bare iron oxide nanoparticles. These results are important due to the application of particular nanoparticles in environmental treatment through deliberately injections of nanoparticles into the wastewater system. Nanoparticles toxicity can be influenced by many factors including size, shape, charge, surface modification and agglomeration

state [177]. Hence, a tiered testing strategy is being encouraged due to the lack of toxicity of iron oxide nanoparticles data available.

Presently, researchers are encouraged to incorporate green chemistry principles to prepare iron oxide-based magnetic nanoparticles to minimize the use of toxic chemical reagents. Green synthesis methods could produce iron oxide nanomaterials which are environmental friendly, safe to human health and sustainable for commercial usage [178]. Besides, the stability of the iron oxide catalyst is a prominent factor from both catalytic and economical viewpoints to prevent adverse effects of transition metals on the receiving environment [179]. The release of soluble iron to the water will decrease its aesthetic quality and result in bad taste, colored, staining, turbidity water and often leads to the problem of red or rusty water at the tap [180].

Photocatalytic degradation of organic pollutants from wastewater using iron oxide nanomaterials will possibility lead to the problem of iron leaching into the treated water. It has been reported that iron oxide dissolution required the breaking of bonds between surface Fe^{3+} and lattice oxygen [181]. Chemical processes that are able to weaken these bonds include protonation of surface sites and photo-reduction of surface sites by reductive agents. When iron oxide absorbs UV light, the excitation of electrons will cause surface Fe^{3+} to be reduced to surface Fe^{2+} states. Then, Fe^{2+} will detach from the iron oxide surface, leaving a vacancy on the oxide surface, which is called surface dissolution [4]. Rodriguez et al. [181] reported that the dissolution rate followed the order of γ-FeOOH > Fe_3O_4 > γ-Fe_2O_3 > α-Fe_2O_3 > α-FeOOH.

According to the United State Environmental Protection Agency, the recommended secondary drinking water regulation for dissolved iron is 0.3 mg/L or below [180]. When iron content is greater than 0.3 mg/L in drinking water, it can cause unpleasant metallic taste and rusty color. Meanwhile, the treated industrial

discharged effluent should meet Standard A (into any inland waters within the catchment areas specified) or B (other inland waters) according to Malaysian Environmental Quality (Sewage Industrial Effluent) Regulations, 2009 depending on the site. The discharge limit of iron content under the Malaysian Environmental Quality Act 1974 for Standard A and B are 1.0 mg/L and 5.0 mg/L, respectively [182].

Majority of the studies found limited iron ions leaching which were about or less than 1 mg/L after photocatalytic reactions [183]. Pastrana-Martínez et al. [184] reported that the maximum load of magnetic nanoparticles that should be used was about 100 mg L^{-1} due to the leaching effect of iron species below 2.0 mg/L. The values of iron leaching was 1.9 mg/L in acidic conditions, <0.1 mg/L in alkaline conditions and the percentage of iron leached remained less than 2.0 mg/L for three catalytic cycles. These values proved that the dissolved iron ions were safely below the limits for wastewater discharge. On the other hand, Belessi et al. [185] found that no photodissolution of iron ions took place as revealed from analysis with inductively coupled plasma mass spectrophotometer. They claimed that the insertion of a protective lining made up of two oppositely charged polyelectrolytes between TiO_2 and γ-Fe_2O_3 inhibited electrical contact and thus prevented photodissolution of the iron oxide phase. Nevertheless, systematic research to examine the stability of iron oxide nanoparticles on various applications is required to avoid iron leaching into the reaction medium and minimize the impact on the environment.

7. Conclusions

Iron oxide magnetic particles possess unique physicochemical properties such as low cost, low toxicity, easy magnetic separation and high surface area. This review

mainly focused on the recent advances in the synthesis, modification and application of iron oxide-based magnetic nanoparticles in the field of photocatalysis. Synthesis methods such as co-precipitation, high-temperature decomposition of organic precursor, hydrothermal, solvothermal and microemulsion approaches have several advantages and disadvantages for preparing iron oxide particles. These synthesis methods show the potential to produce high quantity and quality of iron oxide magnetic particles in a controlled manner and the detailed understanding about the formation mechanism still remained as a challenge. Moreover, more research works should be focused on the suitable method to produce larger scale iron oxide particles rather than sub-gram quantity.

Extensive research has been focused on the enhancement of photocatalysis by modification of iron oxide particles such as geometry morphologies, impurity doping, metal or non-metal loading, coupling with other semiconductors or encapsulation of iron oxide. The current main challenge is the lack of a set of rules or guidelines for the design and synthesis of the optimum magnetic photocatalyst. Researchers should consider the factor of heterojuction between metal oxides composites in terms of the types and percentages of the components in order to maximize the catalytic activity. Excessive metals or support materials can lead to a serious shading effect on the photosentisive catalyst surface, which block the absorption of the incident light and in turn lessen the photocatalytic activity.

The modification of iron oxide-based magnetic nanoparticles in various ways to influence the photocatalytic activities of the catalyst and catalytic reaction mechanism are also reviewed. However, surface modification of particles requires additional steps during preparation method and may decrease the saturation magnetization of the resultant magnetic materials. Hence, one of the major challenges is the design of

magnetic nanoparticles with effective surface modification that provide optimum performance for environmental applications in a sustainable way. Hierarchical self-assembly of nanostructures with various morphologies, design and orientation open a new pathway in environmental materials. Additional challenge is related to the toxicity issues of the production of iron oxide-based magnetic particles.

It should be bear in mind that newly modified magnetic particles need to exhibit excellent magnetic properties for catalytic recyclable usage. Although comparisons between different studies are difficult due to different testing equipment and photocatalytic applications, the universal use of synergy factor and reporting of illumination wavelength are believed able to allow more facile assessment of photocatalytic enhancement. Hence, further development and endorsement of standardised testing methods is required for various applications such as organic pollutant degradation or water splitting in order to achieve a more mature field of research.

Acknowledgement

The authors would like to gratefully acknowledge the financial support provided by the UTAR Research Fund through the Centre for Environment and Green Technology (CEGT), High Impact Research (HIR) Grant from University of Malaya and Fundamental Research Grant Scheme by the Ministry of Education (MOE) Malaysia.

References

[1] X. Feng, H. Guo, K. Patel, H. Zhou, X. Lou, High performance, recoverable Fe_3O_4–ZnO nanoparticles for enhanced photocatalytic degradation of phenol, Chem. Eng. J. 244 (2014) 327-334.

[2] Z. Zhang, M.F. Hossain, T. Takahashi, Self-assembled hematite (α-Fe_2O_3) nanotube arrays for photoelectrocatalytic degradation of azo dye under simulated solar light irradiation, Appl. Catal., B 95 (2010) 423-429.

[3] A. Ghicov, P. Schmuki, Self-ordering electrochemistry: A review on growth and functionality of TiO_2 nanotubes and other self-aligned MO_x structures, Chem. Commun. (2009) 2791-2808.

[4] J. Bandara, U. Klehm, J. Kiwi, Raschig rings-Fe_2O_3 composite photocatalyst activate in the degradation of 4-chlorophenol and Orange II under daylight irradiation, Appl. Catal., B 76 (2007) 73-81.

[5] Y. Cong, M. Chen, T. Xu, Y. Zhang, Q. Wang, Tantalum and aluminum co-doped iron oxide as a robust photocatalyst for water oxidation, Appl. Catal., B 147 (2014) 733-740.

[6] G.K. Pradhan, N. Sahu, K.M. Parida, Fabrication of S, N co-doped α-Fe_2O_3 nanostructures: Effect of doping, OH radical formation, surface area, [110] plane and particle size on the photocatalytic activity, RSC Adv. 3 (2013) 7912-7920.

[7] D. Gumy, S.A. Giraldo, J. Rengifo, C. Pulgarin, Effect of suspended TiO_2 physicochemical characteristics on benzene derivatives photocatalytic degradation, Appl. Catal., B 78 (2008) 19-29.

[8] C. Wang, Y. Ao, P. Wang, J. Hou, J. Qian, A facile method for the preparation of titania-coated magnetic porous silica and its photocatalytic activity under UV or visible light, Colloids Surf. A 360 (2010) 184-189.

[9] M.F.J. Dijkstra, A. Michorius, H. Buwalda, H.J. Panneman, J.G.M. Winkelman, A.A.C.M. Beenackers, Comparison of the efficiency of immobilized and

suspended systems in photocatalytic degradation, Catal. Today 66 (2001) 487-494.

[10] V.M. Daskalaki, Z. Frontistis, D. Mantzavinos, A. Katsaounis, Solar light-induced degradation of bisphenol-A with TiO_2 immobilized on Ti, Catal. Today 161 (2011) 110-114.

[11] S.Q. Li, M.F. Wang, Z.A. Zhu, Q. Wang, X. Zhang, H.Q. Song, D.Q. Cang, Application of superconducting HGMS technology on turbid wastewater treatment from converter, Sep. Purif. Technol. 84 (2012) 56-62.

[12] T. Oka, H. Kanayama, S. Fukui, J. Ogawa, T. Sato, M. Ooizumi, T. Terasawa, Y. Itoh, R. Yabuno, Application of HTS bulk magnet system to the magnetic separation techniques for water purification, Physica C: Superconductivity 468 (2008) 2128-2132.

[13] P.R. Gogate, A.B. Pandit, A review of imperative technologies for wastewater treatment I: Oxidation technologies at ambient conditions, Adv. Environ. Res. 8 (2004) 501-551.

[14] S. Alibeigi, M.R. Vaezi, Phase transformation of iron oxide nanoparticles by varying the molar ratio of Fe^{2+}:Fe^{3+}, Chem. Eng. Technol. 31 (2008) 1591-1596.

[15] D. Arndt, V. Zielasek, W. Dreher, M. Bäumer, Ethylene diamine-assisted synthesis of iron oxide nanoparticles in high-boiling polyolys, J. Colloid Interface Sci. 417 (2014) 188-198.

[16] D. Wang, P. Yang, Y. Zhu, Growth of Fe_3O_4 nanoparticles with tunable sizes and morphologies using organic amine, Mater. Res. Bull. 49 (2014) 514-520.

[17] C.Y. Haw, F. Mohamed, C.H. Chia, S. Radiman, S. Zakaria, N.M. Huang, H.N. Lim, Hydrothermal synthesis of magnetite nanoparticles as MRI contrast agents, Ceram. Int. 36 (2010) 1417-1422.

[18] S.R. Kumar, M.M. Raja, D. Mangalaraj, C. Viswanathan, N. Ponpandian, Surfactant free solvothermal synthesis of monodispersed 3D hierarchical Fe_3O_4 microspheres, Mater. Lett. 110 (2013) 98-101.

[19] Y. Li, R. Jiang, T. Liu, H. Lv, L. Zhou, X. Zhang, One-pot synthesis of grass-like Fe_3O_4 nanostructures by a novel microemulsion-assisted solvothermal method, Ceram. Int. 40 (2014) 1059-1063.

[20] Y.-W. Choi, H. Lee, Y. Song, D. Sohn, Colloidal stability of iron oxide nanoparticles with multivalent polymer surfactants, J. Colloid and Interface Sci. 443 (2015) 8-12.

[21] P.I.P. Soares, A.M.R. Alves, L.C.J. Pereira, J.T. Coutinho, I.M.M. Ferreira, C.M.M. Novo, J.P.M.R. Borges, Effects of surfactants on the magnetic properties of iron oxide colloids, J. Colloid Interface Sci. 419 (2014) 46-51.

[22] J.S. Nunes, C.L. de Vasconcelos, F.A.O. Cabral, J.H. de Araújo, M.R. Pereira, J.L.C. Fonseca, Synthesis and characterization of poly(ethyl methacrylate-co-methacrylic acid) magnetic particles via miniemulsion polymerization, Polymer 47 (2006) 7646-7652.

[23] J.S. Lee, J. Jang, Hetero-structured semiconductor nanomaterials for photocatalytic applications, J. Ind. Eng. Chem. 20 (2014) 363-371.

[24] S. Shylesh, V. Schünemann, W.R. Thiel, Magnetically separable nanocatalysts: Bridges between homogeneous and heterogeneous catalysis, Angew. Chem. Int. Ed. 49 (2010) 3428-3459.

[25] W. Tang, Q. Li, S. Gao, J.K. Shang, Arsenic (III,V) removal from aqueous solution by ultrafine α-Fe_2O_3 nanoparticles synthesized from solvent thermal method, J. Hazard. Mater. 192 (2011) 131-138.

[26] Y. Cudennec, A. Lecerf, Topotactic transformations of goethite and lepidocrocite into hematite and maghemite, Solid State Sci. 7 (2005) 520-529.

[27] J.M. Bigham, R.W. Fitzpatrick, D.G. Schulze, Iron oxides, in: J.B. Dixon, D.G. Schulze (Eds.) Soil Mineralogy with Environmental Applications, Soil Sci. Soc. Am. Book Ser. 2002, pp. 323-366.

[28] M.M. Can, M. Coşkun, T. Fırat, A comparative study of nanosized iron oxide particles; magnetite (Fe_3O_4), maghemite (γ-Fe_2O_3) and hematite (α-Fe_2O_3), using ferromagnetic resonance, J. Alloys Compd. 542 (2012) 241-247.

[29] Z. Jia, J. Liu, Q. Wang, S. Li, Q. Qi, R. Zhu, Synthesis of 3D hierarchical porous iron oxides for adsorption of Congo red from dye wastewater, J. Alloys Compd. 622 (2014) 587-595.

[30] M. Tadic, N. Citakovic, M. Panjan, B. Stanojevic, D. Markovic, Đ. Jovanovic, V. Spasojevic, Synthesis, morphology and microstructure of pomegranate-like hematite (α-Fe_2O_3) superstructure with high coercivity, J. Alloys Compd. 543 (2012) 118-124.

[31] D. Ramimoghadam, S. Bagheri, S.B.A. Hamid, Progress in electrochemical synthesis of magnetic iron oxide nanoparticles, J. Magn. Magn. Mater. 368 (2014) 207-229.

[32] A.-H. Lu, E.L. Salabas, F. Schüth, Magnetic nanoparticles: Synthesis, protection, functionalization, and application, Angew. Chem. Int. Ed. 46 (2007) 1222-1244.

[33] S.-Q. Liu, Magnetic nano-photocatalysts: Preparation, structure, and application, in: E. Lichtfouse, J. Schwarzbauer, D. Robert (Eds.), Environmental Chemistry for a Sustainable World, Springer, Netherlands, 2012, pp. 99-117.

[34] R.D. Ambashta, M. Sillanpää, Water purification using magnetic assistance: A review, J. Hazard. Mater. 180 (2010) 38-49.

[35] Y.A. Koksharov, Magnetism of nanoparticles: Effects of size, shape, and interactions, in: S. P. Gubin (Ed.), Magnetic Nanoparticles, Wiley-VCH Verlag GmbH & Co. KGaA, Weinheim, Germany, 2009, pp. 197-254.

[36] A. Akbarzadeh, M. Samiei, S. Davaran, Magnetic nanoparticles: Preparation, physical properties, and applications in biomedicine, Nanoscale Res. Lett. 7 (2012).

[37] R.M. Cornell and U. Schwertmann, Electronic, electrical and magnetic properties and colour, in The Iron Oxides: Structure, Properties, Reactions, Occurences and Uses, second ed., Wiley-VCH Verlag GmbH & Co. KGaA, Weinheim, 2003, pp. 111-137.

[38] I. Sharifi, H. Shokrollahi, S. Amiri, Ferrite-based magnetic nanofluids used in hyperthermia applications, J. Magn. Magn. Mater. 324 (2012) 903-915.

[39] B. Tang, G. Wang, L. Zhuo, J. Ge, L. Cui, Facile route to α-FeOOH and α-Fe_2O_3 nanorods and magnetic property of α-Fe_2O_3 nanorods, Inorg. Chem. 45 (2006) 5196-5200.

[40] C. Wu, P. Yin, X. Zhu, C. OuYang, Y. Xie, Synthesis of hematite (α-Fe_2O_3) nanorods: Diameter-size and shape effects on their applications in magnetism, lithium ion battery, and gas sensors, J. Phys. Chem. B 110 (2006) 17806-17812.

[41] A.S. Teja, P.Y. Koh, Synthesis, properties, and applications of magnetic iron oxide nanoparticles, Prog. Cryst. Growth Charact. Mater. 55 (2009) 22-45.

[42] D. Ho, X. Sun, S. Sun, Monodisperse magnetic nanoparticles for theranostic applications, Acc. Chem. Res. 44 (2011) 875-882.

[43] Q.A. Pankhurst, J. Connolly, S.K. Jones, J. Dobson, Applications of magnetic nanoparticles in biomedicine, J. Phys. D: Appl. Phys. 36 (2003) R167-R181.

[44] V. Polshettiwar, R. Luque, A. Fihri, H. Zhu, M. Bouhrara, J.M. Basset, Magnetically recoverable nanocatalysts, Chem. Rev. 111 (2011) 3036-3075.

[45] C.V. Vedavyasan, Potential use of magnetic fields - A perspective, Desalination, 134 (2001) 105-108.

[46] B. Liu, B. Gao, X. Xu, W. Hong, Q. Yue, Y. Wang, Y. Su, The combined use of magnetic field and iron-based complex in advanced treatment of pulp and paper wastewater, Chem. Eng. J. 178 (2011) 232-238.

[47] N.S. Zaidi, J. Sohaili, K. Muda, M. Sillanpää, Magnetic field application and its potential in water and wastewater treatment systems, Sep. Purif. Rev. 43 (2014) 206-240.

[48] T. Ohara, H. Kumakura, H. Wada, Magnetic separation using superconducting magnets, Phys. C 357-360 (2001) 1272-1280.

[49] A.K. Gupta, M. Gupta, Synthesis and surface engineering of iron oxide nanoparticles for biomedical applications, Biomaterials 26 (2005) 3995-4021.

[50] G. Salas, R. Costo, M.d.P. Morales, Chapter 2 - Synthesis of inorganic nanoparticles, in: M.d.l.F. Jesus, V. Grazu (Eds.) Frontiers of Nanoscience, Elsevier 2012, pp. 35-79.

[51] W. Wu, Q. He, C. Jiang, Magnetic iron oxide nanoparticles: Synthesis and surface functionalization strategies, Nanoscale Res. Lett. 3 (2008) 397-415.

[52] S.M. El-Sheikh, F.A. Harraz, K.S. Abdel-Halim, Catalytic performance of nanostructured iron oxides synthesized by thermal decomposition technique, J. Alloys Compd. 487 (2009) 716-723.

[53] F. Ozel, H. Kockar, Growth and characterizations of magnetic nanoparticles under hydrothermal conditions: Reaction time and temperature, J. Magn. Magn. Mater. 373 (2015) 213-216.

[54] G. Zhang, Y. Liao, I. Baker, Surface engineering of core/shell iron/iron oxide nanoparticles from microemulsions for hyperthermia, Mater. Sci. Eng.: C 30 (2010) 92-97.

[55] X.M. Li, G. Xu, Y. Liu, T. He, Magnetic Fe_3O_4 nanoparticles: Synthesis and application in water treatment, Nanosci. Nanotechnol.-Asia 1 (2011) 14-24.

[56] T. Otake, D.J. Wesolowski, L.M. Anovitz, L.F. Allard, H. Ohmoto, Experimental evidence for non-redox transformations between magnetite and hematite under H_2-rich hydrothermal conditions, Earth Planet. Sci. Lett. 257 (2007) 60-70.

[57] N. Mahmed, O. Heczko, A. Lancok, S.P. Hannula, The magnetic and oxidation behavior of bare and silica-coated iron oxide nanoparticles synthesized by reverse co-precipitation of ferrous ion (Fe^{2+}) in ambient atmosphere, J. Magn. Magn. Mater. 353 (2014) 15-22.

[58] J. Jing, Y. Zhang, J. Liang, Q. Zhang, E. Bryant, C. Avendano, V. Colvin, Y. Wang, W. Li, W. Yu, One-step reverse precipitation synthesis of water-dispersible superparamagnetic magnetite nanoparticles, J. Nanopart. Res. 14 (2012) 1-8.

[59] A. Ahniyaz, G.A. Seisenbaeva, L. Häggström, S. Kamali, V.G. Kessler, P. Nordblad, C. Johansson, L. Bergström, Preparation of iron oxide nanocrystals by surfactant-free or oleic acid-assisted thermal decomposition of a Fe(III) alkoxide, J. Magn. Magn. Mater. 320 (2008) 781-787.

[60] D. Amara, J. Grinblat, S. Margel, Solventless thermal decomposition of ferrocene as a new approach for one-step synthesis of magnetite nanocubes and nanospheres, J. Mater. Chem. 22 (2012) 2188-2195.

[61] S. Sun, H. Zeng, Size-controlled synthesis of magnetite nanoparticles, J. Am. Chem. Soc. 124 (2002) 8204-8205.

[62] W.W. Yu, J.C. Falkner, C.T. Yavuz, V.L. Colvin, Synthesis of monodisperse iron oxide nanocrystals by thermal decomposition of iron carboxylate salts, Chem. Commun. 10 (2004) 2306-2307.

[63] G.K. Soon, Y. Piao, J. Park, S. Angappane, Y. Jo, N.M. Hwang, J.G. Park, T. Hyeon, Kinetics of monodisperse iron oxide nanocrystal formation by "heating-up" process, J. Am. Chem. Soc. 129 (2007) 12571-12584.

[64] S. Singhal, A.N. Garg, K. Chandra, Synthesis of tris(N,N'-dialkyldithiocarbamato) iron(III) complexes and their thermal decomposition studies by various techniques, J. Alloys Compd. 428 (2007) 72-78.

[65] M. Ştefănescu, O. Ştefănescu, M. Stoia, C. Lazau, Thermal decomposition of some metal-organic precursors, J. Therm. Anal. Calorim. 88 (2007) 27-32.

[66] U. Srivastava, S.K. Kawatra, T.C. Eisele, Production of pig iron by utilizing biomass as a reducing agent, Int. J. Miner. Process. 119 (2013) 51-57.

[67] J.H. Jang, D.E. Lee, M.Y. Kim, H.G. Kim, Investigation of the slab heating characteristics in a reheating furnace with the formation and growth of scale on the slab surface, Int. J. Heat Mass Transfer 53 (2010) 4326-4332.

[68] F. Jay, V. Gauthier-Brunet, F. Pailloux, J. Mimault, S. Bucher, S. Dubois, Al-coated iron particles: Synthesis, characterization and improvement of oxidation resistance, Surf. Coat. Technol. 202 (2008) 4302-4306.

[69] A.P. Herrera, L. Polo-Corrales, E. Chavez, J. Cabarcas-Bolivar, O.N.C. Uwakweh, C. Rinaldi, Influence of aging time of oleate precursor on the magnetic relaxation of cobalt ferrite nanoparticles synthesized by the thermal decomposition method, J. Magn. Magn. Mater. 328 (2013) 41-52.

[70] S.M. El-Sheikh, F.A. Harraz, K.S. Abdel-Halim, Catalytic performance of nanostructured iron oxides synthesized by thermal decomposition technique, J. Alloys Compd. 487 (2009) 716-723.

[71] R. Snovski, J. Grinblat, M.-T. Sougrati, J.-C. Jumas, S. Margel, Synthesis and characterization of iron, iron oxide and iron carbide nanostructures, J. Magn. Magn. Mater. 349 (2014) 35-44.

[72] Z. Weiwei, T. Kaibin, Z. Suyuan, Q. Yunxia, Room temperature synthesis of rod-like $FeC_2O_4 \cdot 2H_2O$ and its transition to maghemite, magnetite and hematite nanorods through controlled thermal decomposition, Nanotechnol. 19 (2008) 065602.

[73] Z. Kozakova, I. Kuritka, P. Bazant, M. Pastorek, V. Babayan, Magnetic needle-like iron oxide particles prepared by microwave-assisted thermal decomposition technique, Mater. Lett. 138 (2015) 116-119.

[74] J. Liu, L. Wang, J. Wang, L. Zhang, Simple solvothermal synthesis of hydrophobic magnetic monodispersed Fe_3O_4 nanoparticles, Mater. Res. Bull. 48 (2013) 416-421.

[75] X. Zhang, Z. Quan, J. Yang, P. Yang, H. Lian, J. Lin, Solvothermal synthesis of well-dispersed $NaMgF_3$ nanocrystals and their optical properties, J. Colloid Interface Sci. 329 (2009) 103-106.

[76] W. Wu, R. Hao, F. Liu, X. Su, Y. Hou, Single-crystalline α-Fe_2O_3 nanostructures: Controlled synthesis and high-index plane-enhanced photodegradation by visible light, J. Mater. Chem. A 1 (2013) 6888-6894.

[77] J. Liang, H. Ma, W. Luo, S. Wang, Synthesis of magnetite submicrospheres with tunable size and superparamagnetism by a facile polyol process, Mater. Chem. Phys. 139 (2013) 383-388.

[78] M. Abbas, B. Parvatheeswara Rao, S.M. Naga, M. Takahashi, C. Kim, Synthesis of high magnetization hydrophilic magnetite (Fe_3O_4) nanoparticles in single reaction–Surfactantless polyol process, Ceram. Int. 39 (2013) 7605-7611.

[79] J.S. Xu, Y.J. Zhu, α-Fe_2O_3 hierarchically hollow microspheres self-assembled with nanosheets: Surfactant-free solvothermal synthesis, magnetic and photocatalytic properties, CrystEngComm 13 (2011) 5162-5169.

[80] F. Hu, K.W. MacRenaris, E.A. Waters, T. Liang, E.A. Schultz-Sikma, A.L. Eckermann, T.J. Meade, Ultrasmall, water-soluble magnetite nanoparticles with high relaxivity for magnetic resonance imaging, J. Phys. Chem. C 113 (2009) 20855-20860.

[81] Q. Guo, P. Guo, J. Li, H. Yin, J. Liu, F. Xiao, D. Shen, N. Li, Fe_3O_4–CNTs nanocomposites: Inorganic dispersant assisted hydrothermal synthesis and application in lithium ion batteries, J. Solid State Chem. 213 (2014) 104-109.

[82] M. Zhu, Y. Wang, D. Meng, X. Qin, G. Diao, Hydrothermal synthesis of hematite nanoparticles and their electrochemical properties, J. Phys. Chem. C 116 (2012) 16276-16285.

[83] J. Liang, L. Li, M. Luo, J. Fang, Y. Hu, Synthesis and properties of magnetite Fe_3O_4 via a simple hydrothermal route, Solid State Sci. 12 (2010) 1422-1425.

[84] M. Shariful Islam, Y. Kusumoto, J. Kurawaki, M. Abdulla-Al-mamun, H. Manaka, A comparative study on heat dissipation, morphological and magnetic properties of hyperthermia suitable nanoparticles prepared by co-precipitation and hydrothermal methods, Bull. Mater. Sci. 35 (2012) 1047-1053.

[85] C. Li, Y. Wei, A. Liivat, Y. Zhu, J. Zhu, Microwave-solvothermal synthesis of Fe_3O_4 magnetic nanoparticles, Mater. Lett. 107 (2013) 23-26.

[86] L. Han, Y. Chen, Y. Wei, Hierarchical flower-like Fe_3O_4 and γ-Fe_2O_3 nanostructures: Synthesis, growth mechanism and photocatalytic properties, CrystEngComm 14 (2012) 4692-4698.

[87] Y.B. Khollam, S.R. Dhage, H.S. Potdar, S.B. Deshpande, P.P. Bakare, S.D. Kulkarni, S.K. Date, Microwave hydrothermal preparation of submicron-sized spherical magnetite (Fe_3O_4) powders, Mater. Lett. 56 (2002) 571-577.

[88] H. Liu, S. Ji, H. Yang, H. Zhang, M. Tang, Ultrasonic-assisted ultra-rapid synthesis of monodisperse meso-SiO_2@Fe_3O_4 microspheres with enhanced mesoporous structure, Ultrason. Sonochem. 21 (2014) 505-512.

[89] T. Aubert, F. Grasset, S. Mornet, E. Duguet, O. Cador, S. Cordier, Y. Molard, V. Demange, M. Mortier, H. Haneda, Functional silica nanoparticles synthesized by water-in-oil microemulsion processes, J. Colloid Interface Sci. 341 (2010) 201-208.

[90] T. Lu, J. Wang, J. Yin, A. Wang, X. Wang, T. Zhang, Surfactant effects on the microstructures of Fe_3O_4 nanoparticles synthesized by microemulsion method, Colloids Surf. A 436 (2013) 675-683.

[91] D. Zhang, Z. Tong, S. Li, X. Zhang, A. Ying, Fabrication and characterization of hollow Fe_3O_4 nanospheres in a microemulsion, Mater. Lett. 62 (2008) 4053-4055.

[92] K. Holmberg, Surfactant-templated nanomaterials synthesis, J. Colloid Interface Sci. 274 (2004) 355-364.

[93] Y. Li, R. Jiang, T. Liu, H. Lv, X. Zhang, Single-microemulsion-based solvothermal synthesis of magnetite microflowers, Ceram. Int. 40 (2014) 4791-4795.

[94] D.S. Mathew, R.-S. Juang, An overview of the structure and magnetism of spinel ferrite nanoparticles and their synthesis in microemulsions, Chem. Eng. J. 129 (2007) 51-65.

[95] H. Zhang, G. Chen, D.W. Bahnemann, Photoelectrocatalytic materials for environmental applications, J. Mater. Chem. 19 (2009) 5089-5121.

[96] M. Kitano, M. Hara, Heterogeneous photocatalytic cleavage of water, J. Mater. Chem. 20 (2010) 627-641.

[97] M. Pelaez, N.T. Nolan, S.C. Pillai, M.K. Seery, P. Falaras, A.G. Kontos, P.S.M. Dunlop, J.W.J. Hamilton, J.A. Byrne, K. O'Shea, M.H. Entezari, D.D. Dionysiou, A review on the visible light active titanium dioxide photocatalysts for environmental applications, Appl. Catal., B 125 (2012) 331-349.

[98] M. Niu, F. Huang, L. Cui, P. Huang, Y. Yu, Y. Wang, Hydrothermal synthesis, structural characteristics, and enhanced photocatalysis of SnO_2/α-Fe_2O_3 semiconductor nanoheterostructures, ACS Nano 4 (2010) 681-688.

[99] C. Karunakaran, S. SakthiRaadha, P. Gomathisankar, Photocatalytic and bactericidal activities of hydrothermally and sonochemically prepared Fe_2O_3–SnO_2 nanoparticles, Mater. Sci. Semicond. Process. 16 (2013) 818-824.

[100] V. Preethi, S. Kanmani, Photocatalytic hydrogen production using Fe_2O_3-based core shell nano particles with ZnS and CdS, Int. J. Hydrogen Energy 39 (2014) 1613-1622.

[101] X. Liu, Z. Fang, X. Zhang, W. Zhang, X. Wei, B. Geng, Preparation and characterization of Fe_3O_4/CdS nanocomposites and their use as recyclable photocatalysts, Cryst. Growth Des. 9 (2009) 197-202.

[102] P. Ju, P. Wang, B. Li, H. Fan, S. Ai, D. Zhang, Y. Wang, A novel calcined Bi_2WO_6/$BiVO_4$ heterojunction photocatalyst with highly enhanced photocatalytic activity, Chem. Eng. J. 236 (2014) 430-437.

[103] S. Hosseini, E. Eftekhari, S.M. Soltani, F.E. Babadi, L.J. Minggu, M.H.S. Ismail, Synthesis, characterization and performance evaluation of three-layered photoanodes by introducing a blend of WO_3 and Fe_2O_3 for dye degradation, Appl. Surf. Sci. 289 (2014) 53-61.

[104] G. Xi, B. Yue, J. Cao, J. Ye, Fe_3O_4/WO_3 Hierarchical core-shell structure: High-performance and recyclable visible-light photocatalysis, Chem. - Eur. J. 17 (2011) 5145-5154.

[105] D. Bi, Y. Xu, Synergism between Fe_2O_3 and WO_3 particles: Photocatalytic activity enhancement and reaction mechanism, J. Mol. Catal. A: Chem. 367 (2013) 103-107.

[106] H. Zhou, C. Zhang, X. Wang, H. Li, Z. Du, Fabrication of TiO_2-coated magnetic nanoparticles on functionalized multi-walled carbon nanotubes and their photocatalytic activity, Synth. Met. 161 (2011) 2199-2205.

[107] J. Young Kim, J.W. Jang, D. Hyun Youn, J. Yul Kim, E. Sun Kim, J. Sung Lee, Graphene-carbon nanotube composite as an effective conducting scaffold to enhance the photoelectrochemical water oxidation activity of a hematite film, RSC Adv. 2 (2012) 9415-9422.

[108] G.K. Pradhan, D.K. Padhi, K.M. Parida, Fabrication of α-Fe_2O_3 Nanorod/RGO composite: A novel hybrid photocatalyst for phenol degradation, ACS Appl. Mater. Interfaces 5 (2013) 9101-9110.

[109] Y. Dong, D. Tang, C. Li, Photocatalytic oxidation of methyl orange in water phase by immobilized TiO_2-carbon nanotube nanocomposite photocatalyst, Appl. Surf. Sci. 296 (2014) 1-7.

[110] D. Ljubas, M. Franzreb, H.C. Bruun Hansen, P.G. Weidler, Magnetizing of nano-materials on example of Degussa's P-25 TiO_2 photocatalyst: Synthesis of magnetic aggregates, characterization and possible use, Sep. Purif. Technol. 136 (2014) 274-285.

[111] H. Park, Y. Park, W. Kim, W. Choi, Surface modification of TiO_2 photocatalyst for environmental applications, J. Photochem. Photobiol. C 15 (2013) 1-20.

[112] J. Lei, C. Liu, F. Li, X. Li, S. Zhou, T. Liu, M. Gu, Q. Wu, Photodegradation of orange I in the heterogeneous iron oxide–oxalate complex system under UVA irradiation, J. Hazard. Mater. 137 (2006) 1016-1024.

[113] J.-W. Shi, H.-J. Cui, J.-W. Chen, M.-L. Fu, B. Xu, H.-Y. Luo, Z.-L. Ye, TiO_2/activated carbon fibers photocatalyst: Effects of coating procedures on the microstructure, adhesion property, and photocatalytic ability, J. Colloid Interface Sci. 388 (2012) 201-208.

[114] S. Bhukal, R. Sharma, S. Mor, S. Singhal, Mg–Co–Zn magnetic nanoferrites: Characterization and their use for remediation of textile wastewater, Superlattices and Microstruct. 77 (2015) 134-151.

[115] P. Olsson, C. Domain, J.F. Guillemoles, Ferromagnetic compounds for high efficiency photovoltaic conversion: The case of AlP:Cr, Phys. Rev. Lett. 102 (2009) 227204.

[116] Y.H. Wang, J.L. Zhao, Y. Liang, Degradation kinetics of phenol by a titanium dioxide photocatalyst coupled with a magnetic field, React. Kinet., Mech. Catal. 109 (2013) 273-283.

[117] T. Xie, L. Xu, C. Liu, Y. Wang, Magnetic composite $ZnFe_2O_4/SrFe_{12}O_{19}$: Preparation, characterization, and photocatalytic activity under visible light, Appl. Surf. Sci. 273 (2013) 684-691.

[118] S. Joonwichien, E. Yamasue, H. Okumura, K.N. Ishihara, Effect of static magnetic field on photocatalytic degradation of Methylene Blue over ZnO and TiO_2 powders, Appl. Magn. Reson. 42 (2012) 17-28.

[119] Y. Zhu, L.P. Stubbs, F. Ho, R. Liu, C.P. Ship, J.A. Maguire, N.S. Hosmane, Magnetic nanocomposites: A new perspective in catalysis, ChemCatChem 2 (2010) 365-374.

[120] S. Briceño, H.D. Castillo, V. Sagredo, W. Bramer-Escamilla, P. Silva, Structural, catalytic and magnetic properties of $Cu_{1-X}Co_XFe_2O_4$, Appl. Surf. Sci. 263 (2012) 100-103.

[121] J. Zhan, H. Zhang, G. Zhu, Magnetic photocatalysts of cenospheres coated with Fe_3O_4/TiO_2 core/shell nanoparticles decorated with Ag nanopartilces, Ceram. Int. 40 (2014) 8547-8559.

[122] G.-D. Fang, D.-M. Zhou, D.D. Dionysiou, Superoxide mediated production of hydroxyl radicals by magnetite nanoparticles: Demonstration in the degradation of 2-chlorobiphenyl, J. Hazard. Mater. 250-251 (2013) 68-75.

[123] G.-D. Fang, D.D. Dionysiou, S.R. Al-Abed, D.-M. Zhou, Superoxide radical driving the activation of persulfate by magnetite nanoparticles: Implications for the degradation of PCBs, Appl. Catal., B 129 (2013) 325-332.

[124] S. Peng, S. Sun, Synthesis and characterization of monodisperse hollow Fe_3O_4 nanoparticles, Angew. Chem. Int. Ed. 46 (2007) 4155-4158.

[125] M. Tadic, S. Kralj, M. Jagodic, D. Hanzel, D. Makovec, Magnetic properties of novel superparamagnetic iron oxide nanoclusters and their peculiarity under annealing treatment, Appl. Surf. Sci. 322 (2014) 255-264.

[126] P.N.R. Kishore, P. Jeevanandam, A novel thermal decomposition approach for the synthesis of silica-iron oxide core-shell nanoparticles, J. Alloys Compd. 522 (2012) 51-62.

[127] J. Yue, X. Jiang, Y.V. Kaneti, A. Yu, Deposition of gold nanoparticles on β-FeOOH nanorods for detecting melamine in aqueous solution, J. Colloid Interface Sci. 367 (2012) 204-212.

[128] H. Liang, X. Jiang, W. Chen, S. Wang, B. Xu, Z. Wang, α-Fe_2O_3/Pt hybrid nanorings and their enhanced photocatalytic activities, Ceram. Int. 40 (2014) 5653-5658.

[129] S. Zeng, K. Tang, T. Li, Z. Liang, Hematite with the urchinlike structure: Its shape-selective synthesis, magnetism, and enhanced photocatalytic performance after TiO_2 encapsulation, J. Phys. Chem. C 114 (2010) 274-283.

[130] Z. Xiao, J. Li, J. Zhong, W. Hu, J. Zeng, S. Huang, X. Lu, J. He, M. Li, Enhanced photocatalytic decolorization of methyl orange by gallium-doped α-Fe_2O_3, Mater. Sci. Semicond. Process. 24 (2014) 104-109.

[131] R. Rahimi, A. Tadjarodi, M. Rabbani, H. Kerdari, M. Imani, Preparation, characterization and photocatalytic properties of Ba-Cd-Sr-Ti doped Fe_3O_4 nanohollow spheres on removal of congo red under visible-light irradiation, J. Supercond. Novel Magn. 26 (2013) 219-228.

[132] S. Yang, Y. Xu, Y. Cao, G. Zhang, Y. Sun, D. Gao, Zn(ii)-doped γ-Fe_2O_3 single-crystalline nanoplates with high phase-transition temperature, superparamagnetic property and good photocatalytic property, RSC Adv. 3 (2013) 21994-22001.

[133] E. Thimsen, F. Le Formal, M. Grätzel, S.C. Warren, Influence of plasmonic Au nanoparticles on the photoactivity of Fe_2O_3 electrodes for water splitting, Nano Lett. 11 (2011) 35-43.

[134] L. Chen, F. Li, B. Ni, J. Xu, Z. Fu, Y. Lu, Enhanced visible photocatalytic activity of hybrid Pt/α-Fe_2O_3 nanorods, RSC Adv. 2 (2012) 10057-10063.

[135] R.Y. Hong, S.Z. Zhang, G.Q. Di, H.Z. Li, Y. Zheng, J. Ding, D.G. Wei, Preparation, characterization and application of Fe_3O_4/ZnO core/shell magnetic nanoparticles, Mater. Res. Bull. 43 (2008) 2457-2468.

[136] L. Zhang, J. Lian, L. Wu, Z. Duan, J. Jiang, L. Zhao, Synthesis of a thin-layer MnO_2 nanosheet-coated Fe_3O_4 nanocomposite as a magnetically separable photocatalyst, Langmuir 30 (2014) 7006-7013.

[137] J. Su, Y. Zhang, S. Xu, S. Wang, H. Ding, S. Pan, G. Wang, G. Li, H. Zhao, Highly efficient and recyclable triple-shelled Ag@Fe_3O_4@SiO_2@TiO_2 photocatalysts for degradation of organic pollutants and reduction of hexavalent chromium ions, Nanoscale, 6 (2014) 5181-5192.

[138] L.-J. Kim, J.-W. Jang, J.-W. Park, Nano TiO_2-functionalized magnetic-cored dendrimer as a photocatalyst, Appl. Catal., B 147 (2014) 973-979.

[139] H. Liang, H. Niu, P. Li, Z. Tao, C. Mao, J. Song, S. Zhang, Multifunctional Fe_3O_4@C@Ag hybrid nanoparticles: Aqueous solution preparation, characterization and photocatalytic activity, Mater. Res. Bull., 48 (2013) 2415-2419.

[140] L. Zhang, W. Wang, M. Shang, S. Sun, J. Xu, Bi_2WO_6@carbon/Fe_3O_4 microspheres: Preparation, growth mechanism and application in water treatment, J. Hazard. Mater. 172 (2009) 1193-1197.

[141] P. Xu, G.M. Zeng, D.L. Huang, C.L. Feng, S. Hu, M.H. Zhao, C. Lai, Z. Wei, C. Huang, G.X. Xie, Z.F. Liu, Use of iron oxide nanomaterials in wastewater treatment: A review, Sci. Total Environ. 424 (2012) 1-10.

[142] L. Guo, F. Chen, X. Fan, W. Cai, J. Zhang, S-doped α-Fe_2O_3 as a highly active heterogeneous Fenton-like catalyst towards the degradation of acid orange 7 and phenol, Appl. Catal., B 96 (2010) 162-168.

[143] N.C. Feitoza, T.D. Gonçalves, J.J. Mesquita, J.S. Menegucci, M.-K.M.S. Santos, J.A. Chaker, R.B. Cunha, A.M.M. Medeiros, J.C. Rubim, M.H. Sousa, Fabrication of glycine-functionalized maghemite nanoparticles for magnetic removal of copper from wastewater, J. Hazard. Mater. 264 (2014) 153-160.

[144] H. Wu, L. Wang, Phase transformation-induced crystal plane effect of iron oxide micropine dendrites on gaseous toluene photocatalytic oxidation, Appl. Surf. Sci. 288 (2014) 398-404.

[145] M. Batzill, Fundamental aspects of surface engineering of transition metal oxide photocatalysts, Energy Environ. Sci. 4 (2011) 3275-3286.

[146] A. Šutka, S. Lagzdina, I. Juhnevica, D. Jakovlevs, M. Maiorov, Precipitation synthesis of magnetite Fe_3O_4 nanoflakes, Ceram. Int. 40 (2014) 11437-11440.

[147] H. Tang, W.J. Yin, M.A. Matin, H. Wang, T. Deutsch, M.M. Al-Jassim, J.A. Turner, Y. Yan, Titanium and magnesium Co-alloyed hematite thin films for photoelectrochemical water splitting, J. Appl. Phys. 111 (2012).

[148] Y.S. Hu, A. Kleiman-Shwarsctein, A.J. Forman, D. Hazen, J.N. Park, E.W. McFarland, Pt-doped α-Fe_2O_3 thin films active for photoelectrochemical water splitting, Chem. Mater. 20 (2008) 3803-3805.

[149] A. Kleiman-Shwarsctein, Y.S. Hu, A.J. Forman, G.D. Stucky, E.W. McFarland, Electrodeposition of α-Fe_2O_3 doped with Mo or Cr as photoanodes for photocatalytic water splitting, J. Phys. Chem. C 112 (2008) 15900-15907.

[150] Y. Wei, S. Han, D.A. Walker, S.C. Warren, B.A. Grzybowski, Enhanced photocatalytic activity of hybrid Fe_2O_3-Pd nanoparticulate catalysts, Chem. Sci. 3 (2012) 1090-1094.

[151] J.S. Jang, K.Y. Yoon, Y. Xiao, F.R.F. Fan, A.J. Bard, Development of a potential Fe_2O_3-based photocatalyst thin film for water oxidation by scanning electrochemical microscopy: Effects of Ag-Fe_2O_3 nanocomposite and Sn doping, Chem. Mater. 21 (2009) 4803-4810.

[152] A. Ramchiary, S.K. Samdarshi, Ag deposited mixed phase titania visible light photocatalyst–Superiority of Ag-titania and mixed phase titania co-junction, Appl. Surf. Sci. 305 (2014) 33-39.

[153] H. Kim, M. Achermann, L.P. Balet, J.A. Hollingsworth, V.I. Klimov, Synthesis and characterization of Co/CdSe core/shell nanocomposites: Bifunctional magnetic-optical nanocrystals, J. Am. Chem. Soc. 127 (2005) 544-546.

[154] D. Beydoun, R. Amal, G. Low, S. McEvoy, Occurrence and prevention of photodissolution at the phase junction of magnetite and titanium dioxide, J. Mol. Catal. A: Chem. 180 (2002) 193-200.

[155] D. Beydoun, R. Amal, G.K.C. Low, S. McEvoy, Novel photocatalyst: Titania-coated magnetite, activity and photodissolution, J. Phys. Chem. B 104 (2000) 4387-4396.

[156] X. Yong, M.A.A. Schoonen, The absolute energy positions of conduction and valence bands of selected semiconducting minerals, Am. Mineral. 85 (2000) 543-556.

[157] M.L. Maya-Treviño, J.L. Guzmán-Mar, L. Hinojosa-Reyes, N.A. Ramos-Delgado, M.I. Maldonado, A. Hernández-Ramírez, Activity of the ZnO–Fe_2O_3 catalyst on the degradation of Dicamba and 2,4-D herbicides using simulated solar light, Ceram. Int. 40 (2014) 8701-8708.

[158] L. Qin, X. Pan, L. Wang, X. Sun, G. Zhang, X. Guo, Facile preparation of mesoporous TiO_2(B) nanowires with well-dispersed Fe_2O_3 nanoparticles and their photochemical catalytic behavior, Appl. Catal., B 150–151 (2014) 544-553.

[159] O. Akhavan, R. Azimirad, Photocatalytic property of Fe_2O_3 nanograin chains coated by TiO_2 nanolayer in visible light irradiation, Appl. Catal., A 369 (2009) 77-82.

[160] J. Jing, J. Li, J. Feng, W. Li, W.W. Yu, Photodegradation of quinoline in water over magnetically separable Fe_3O_4/TiO_2 composite photocatalysts, Chem. Eng. J. 219 (2013) 355-360.

[161] L. Zhang, W. Wang, L. Zhou, M. Shang, S. Sun, Fe_3O_4 coupled BiOCl: A highly efficient magnetic photocatalyst, Appl. Catal., B 90 (2009) 458-462.

[162] N. Shpaisman, E.R. Bauminger, S. Margel, One-step synthesis of air-stable nanocrystalline iron particles by thermal decomposition of triiron dodecacarbonyl, J. Alloys Compd. 454 (2008) 89-96.

[163] J.P. Cheng, R. Ma, M. Li, J.S. Wu, F. Liu, X.B. Zhang, Anatase nanocrystals coating on silica-coated magnetite: Role of polyacrylic acid treatment and its photocatalytic properties, Chem. Eng. J. 210 (2012) 80-86.

[164] N. Ferroudj, J. Nzimoto, A. Davidson, D. Talbot, E. Briot, V. Dupuis, A. Bée, M.S. Medjram, S. Abramson, Maghemite nanoparticles and maghemite/silica nanocomposite microspheres as magnetic Fenton catalysts for the removal of water pollutants, Appl. Catal., B 136–137 (2013) 9-18.

[165] Y.-H. Deng, C.-C. Wang, J.-H. Hu, W.-L. Yang, S.-K. Fu, Investigation of formation of silica-coated magnetite nanoparticles via sol–gel approach, Colloids Surf., A 262 (2005) 87-93.

[166] Z. Wang, H. Guo, Y. Yu, N. He, Synthesis and characterization of a novel magnetic carrier with its composition of Fe_3O_4/carbon using hydrothermal reaction, J. Magn. Magn. Mater. 302 (2006) 397-404.

[167] M. Inagaki, Carbon coating for enhancing the functionalities of materials, Carbon 50 (2012) 3247-3266.

[168] Y. Liu, L. Zhou, Y. Hu, C. Guo, H. Qian, F. Zhang, X.W. Lou, Magnetic-field induced formation of 1D Fe_3O_4/C/CdS coaxial nanochains as highly efficient and reusable photocatalysts for water treatment, J. Mater. Chem. 21 (2011) 18359-18364.

[169] Y. Cheng, F. Gao, L. An, X. Li, G. Wang, Different combinations of Fe_3O_4 microsphere, Polypyrrole and silver as core-shell nanocomposites for adsorption and photocatalytic application, Adv. Powder Technol. 25 (2014) 1600-1607.

[170] X. Guo, Y. Deng, D. Gu, R. Che, D. Zhao, Synthesis and microwave absorption of uniform hematite nanoparticles and their core-shell mesoporous silica nanocomposites, J. Mater. Chem. 19 (2009) 6706-6712.

[171] X. Lu, M. Niu, R. Qiao, M. Gao, Superdispersible PVP-coated Fe_3O_4 nanocrystals prepared by a "one-pot" reaction, J. Phys. Chem. B 112 (2008) 14390-14394.

[172] Z. Lu, F. Chen, M. He, M. Song, Z. Ma, W. Shi, Y. Yan, J. Lan, F. Li, P. Xiao, Microwave synthesis of a novel magnetic imprinted TiO_2 photocatalyst with excellent transparency for selective photodegradation of enrofloxacin hydrochloride residues solution, Chem. Eng. J. 249 (2014) 15-26.

[173] Y. Wang, H. Sun, X. Duan, H.M. Ang, M.O. Tadé, S. Wang, A new magnetic nano zero-valent iron encapsulated in carbon spheres for oxidative degradation of phenol, Appl. Catal., B 172–173 (2015) 73-81.

[174] M. Farré, K. Gajda-Schrantz, L. Kantiani, D. Barceló, Ecotoxicity and analysis of nanomaterials in the aquatic environment, Anal. Bioanal. Chem. 393 (2009) 81-95.

[175] S. Liu, Y. Han, L. Yin, L. Long, R. Liu, Toxicology studies of a superparamagnetic iron oxide nanoparticle in vivo, Adv. Mater. Res. 47-50 (2008) 1097-1100.

[176] M. Mahmoudi, A. Simchi, M. Imani, M.A. Shokrgozar, A.S. Milani, U.O. Häfeli, P. Stroeve, A new approach for the in vitro identification of the cytotoxicity of superparamagnetic iron oxide nanoparticles, Colloids Surf., B 75 (2010) 300-309.

[177] M. Mahmoudi, H. Hosseinkhani, M. Hosseinkhani, S. Boutry, A. Simchi, W. Shane Journeay, K. Subramani, S. Laurent, Magnetic resonance imaging tracking of stem cells in vivo using iron oxide nanoparticles as a tool for the advancement of clinical regenerative medicine, Chem. Rev. 111 (2011) 253-280.

[178] H.C. Genuino, N. Mazrui, M.S. Seraji, Z. Luo, G.E. Hoag, Chapter 3 - Green synthesis of iron nanomaterials for oxidative catalysis of organic environmental pollutants, in: S.L. Suib (Ed.) New and Future Developments in Catalysis, Elsevier, Amsterdam, 2013, pp. 41-61.

[179] S. Rahim Pouran, A.A. Abdul Raman, W.M.A. Wan Daud, Review on the application of modified iron oxides as heterogeneous catalysts in Fenton reactions, J. Cleaner Prod. 64 (2014) 24-35.

[180] M.S. Rahman, G.A. Gagnon, Bench-scale evaluation of drinking water treatment parameters on iron particles and water quality, Water Res. 48 (2014) 137-147.

[181] E. Rodríguez, G. Fernández, B. Ledesma, P. Álvarez, F.J. Beltrán, Photocatalytic degradation of organics in water in the presence of iron oxides: Influence of carboxylic acids, Appl. Catal., B 92 (2009) 240-249.

[182] Department of Environment Malaysia (DOE), Environmental Quality Act 1974 (Act 127), 1974.

[183] M. Minella, G. Marchetti, E. De Laurentiis, M. Malandrino, V. Maurino, C. Minero, D. Vione, K. Hanna, Photo-Fenton oxidation of phenol with magnetite as iron source, Appl. Catal., B 154-155 (2014) 102-109.

[184] L.M. Pastrana-Martínez, N. Pereira, R. Lima, J.L. Faria, H.T. Gomes, A.M.T. Silva, Degradation of diphenhydramine by photo-Fenton using magnetically recoverable iron oxide nanoparticles as catalyst, Chem. Eng. J. 261 (2014) 45-52.

[185] V. Belessi, D. Lambropoulou, I. Konstantinou, R. Zboril, J. Tucek, D. Jancik, T. Albanis, D. Petridis, Structure and photocatalytic performance of magnetically separable titania photocatalysts for the degradation of propachlor, Appl. Catal., B 87 (2009) 181-189.

List of Figures

List of Tables

Fig. 1

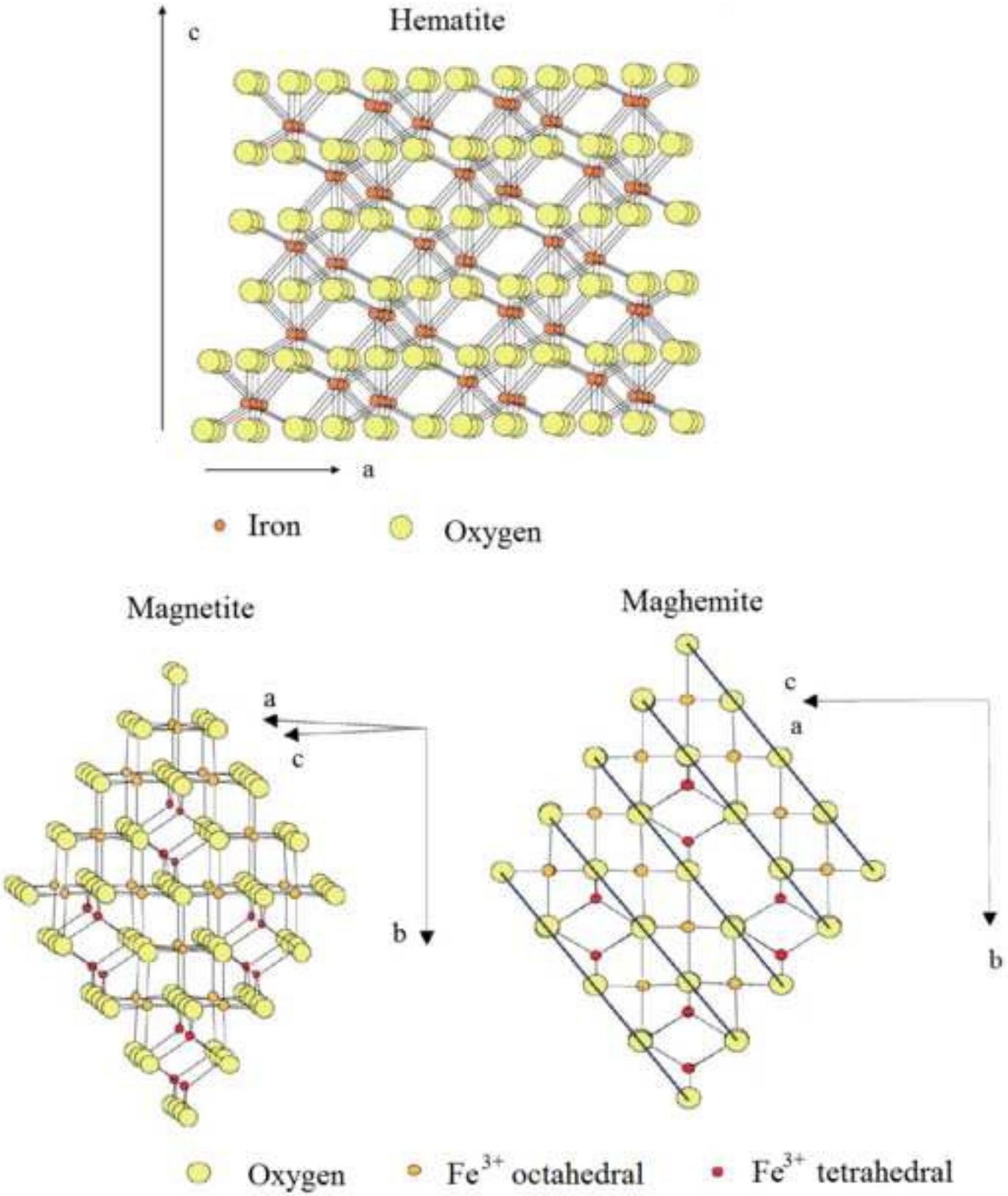

Fig. 2

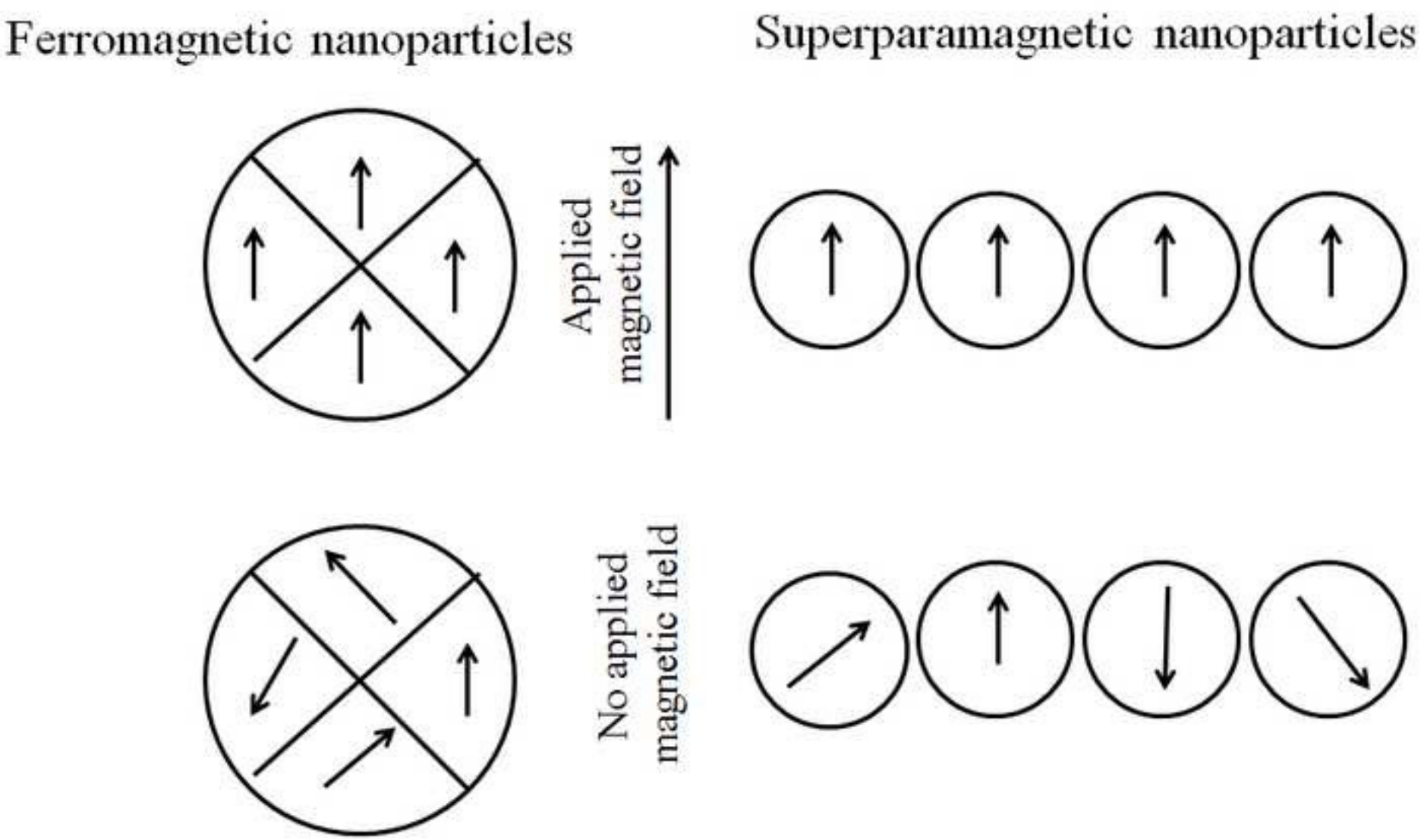

Fig. 3

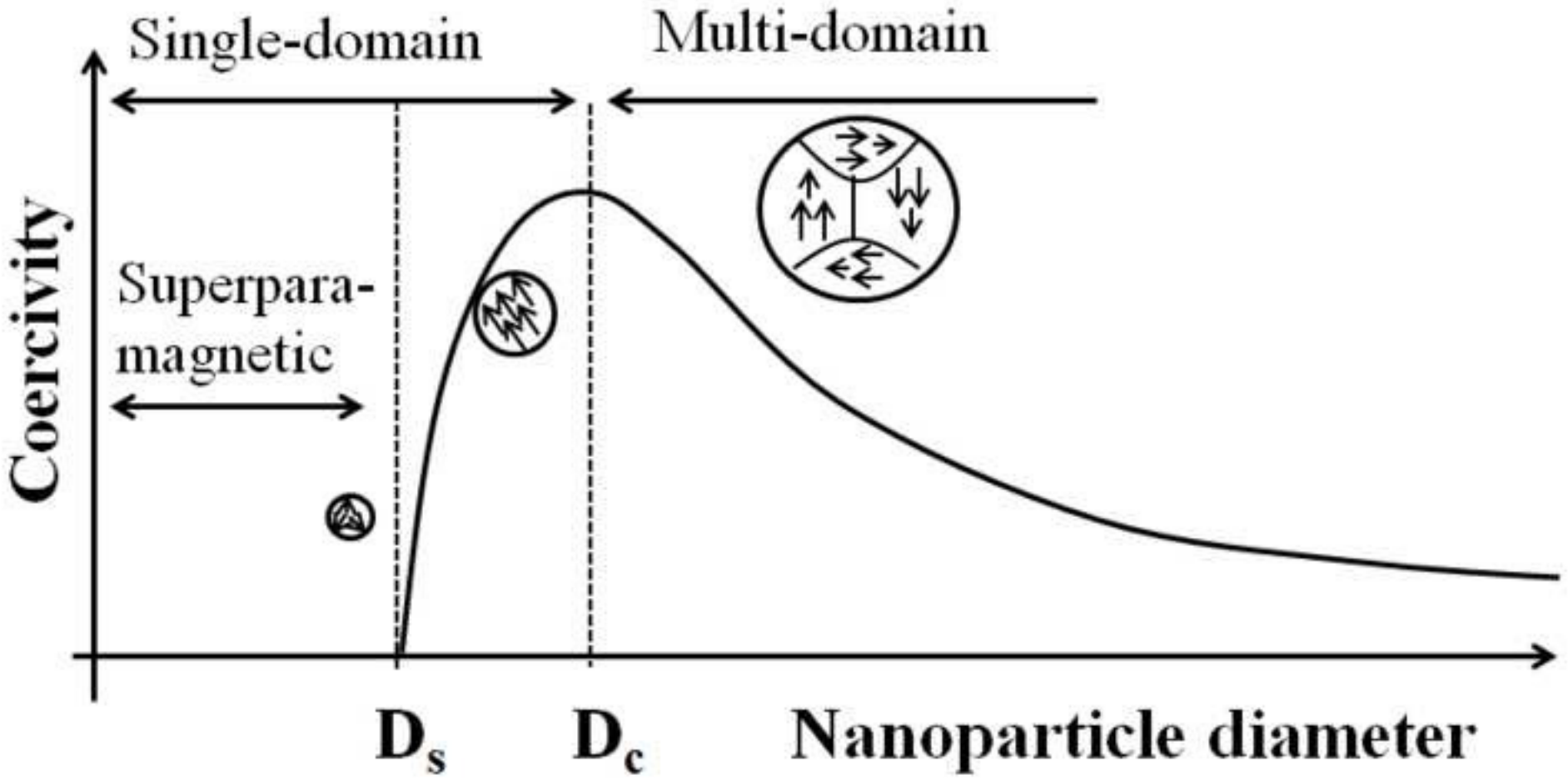

D_s: Superparamagnetism size threshold

D_c : Critical size threshold

Fig. 4

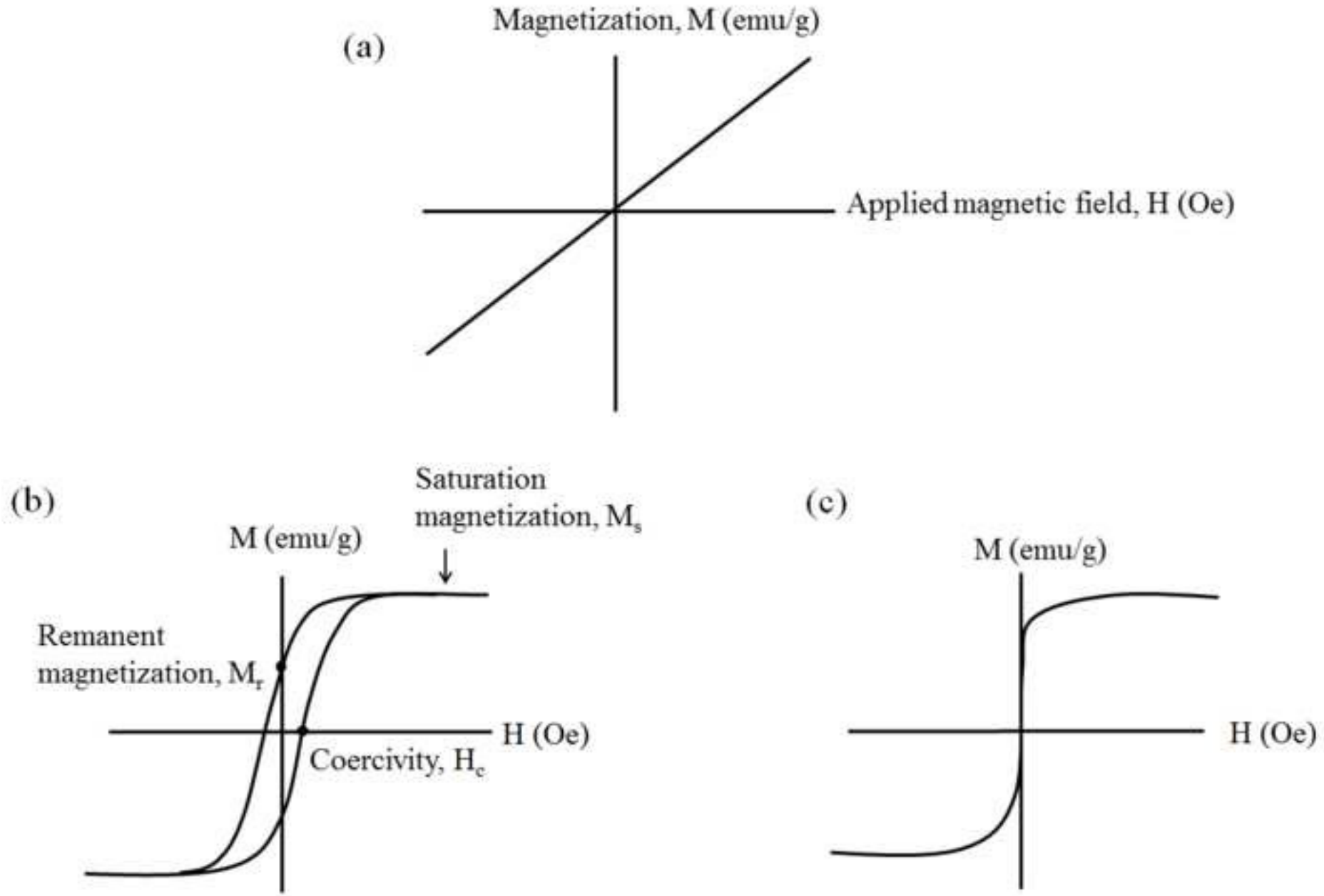

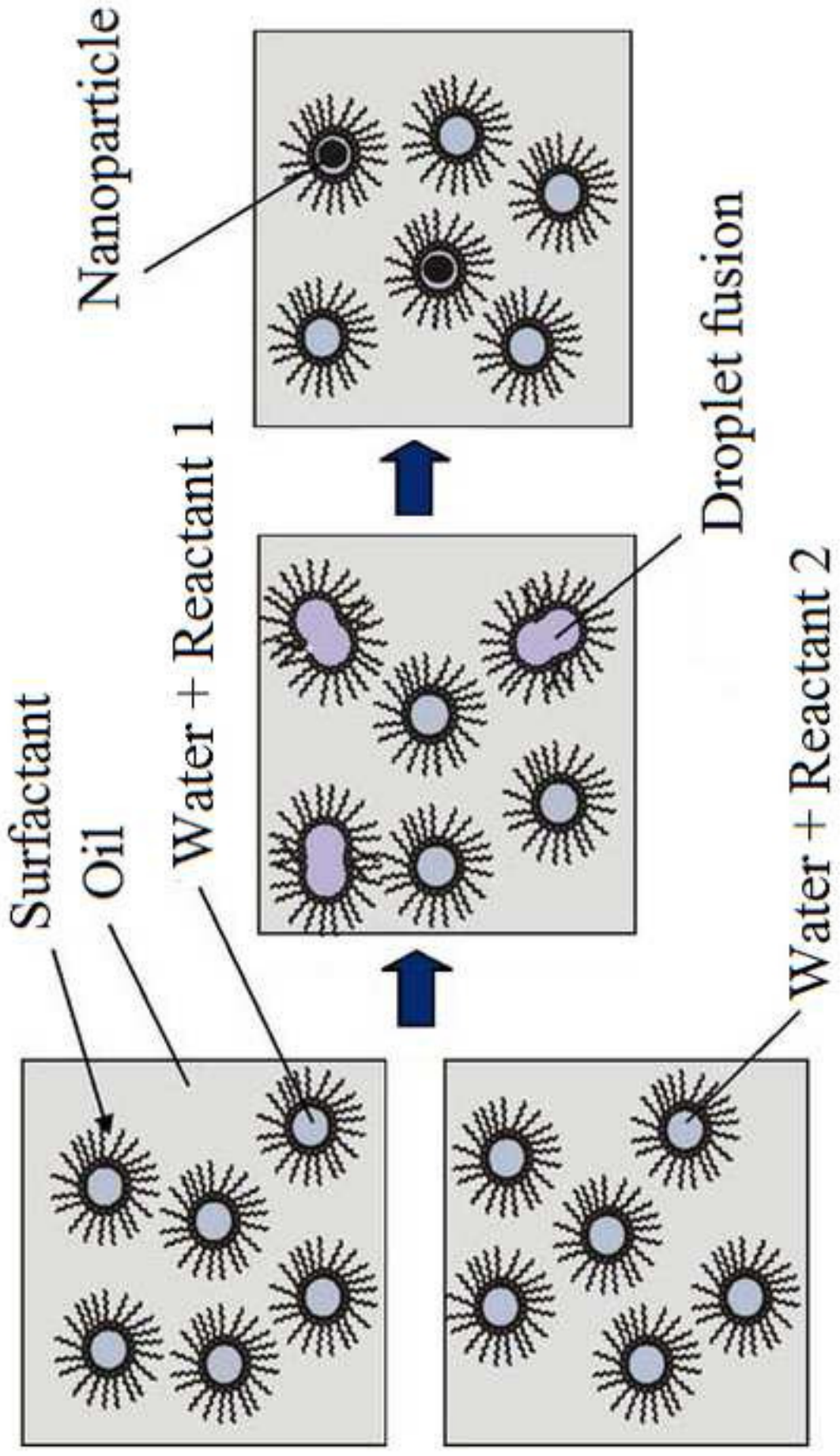
Nanoparticle
Surfactant
Oil
Water + Reactant 1
Droplet fusion
Water + Reactant 2

Fig. 5

Fig. 6

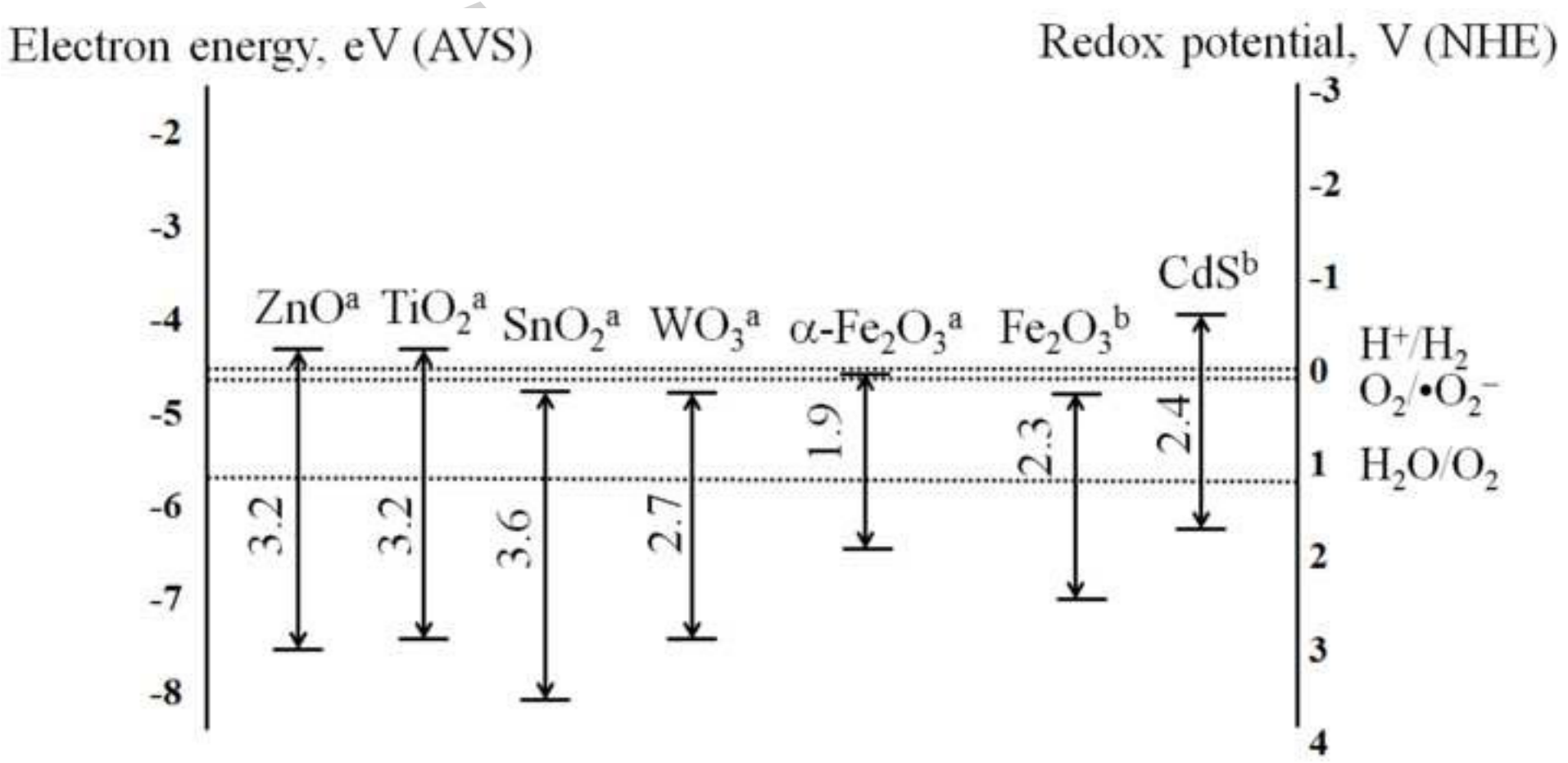

Fig. 7

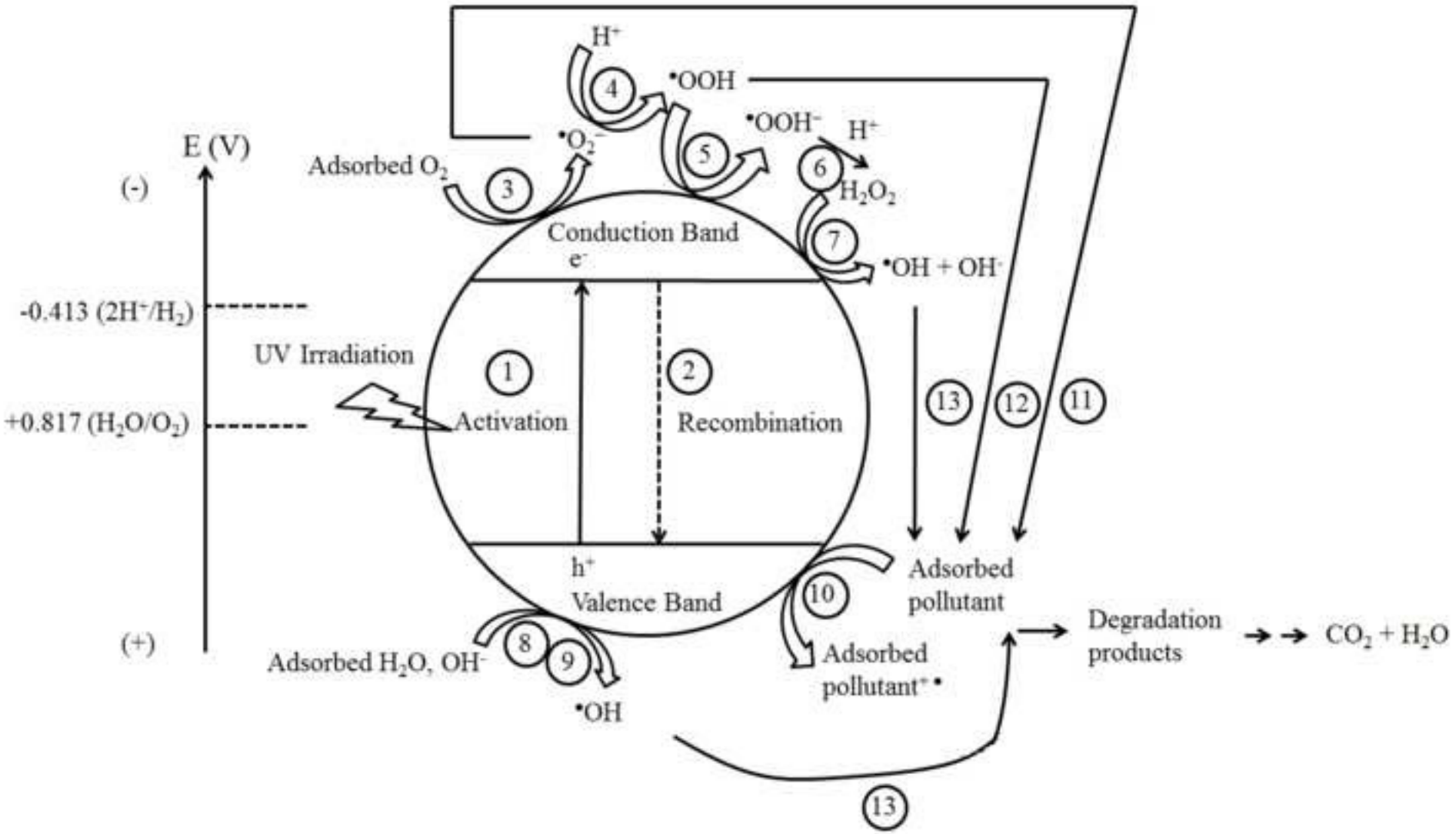

Fig. 8

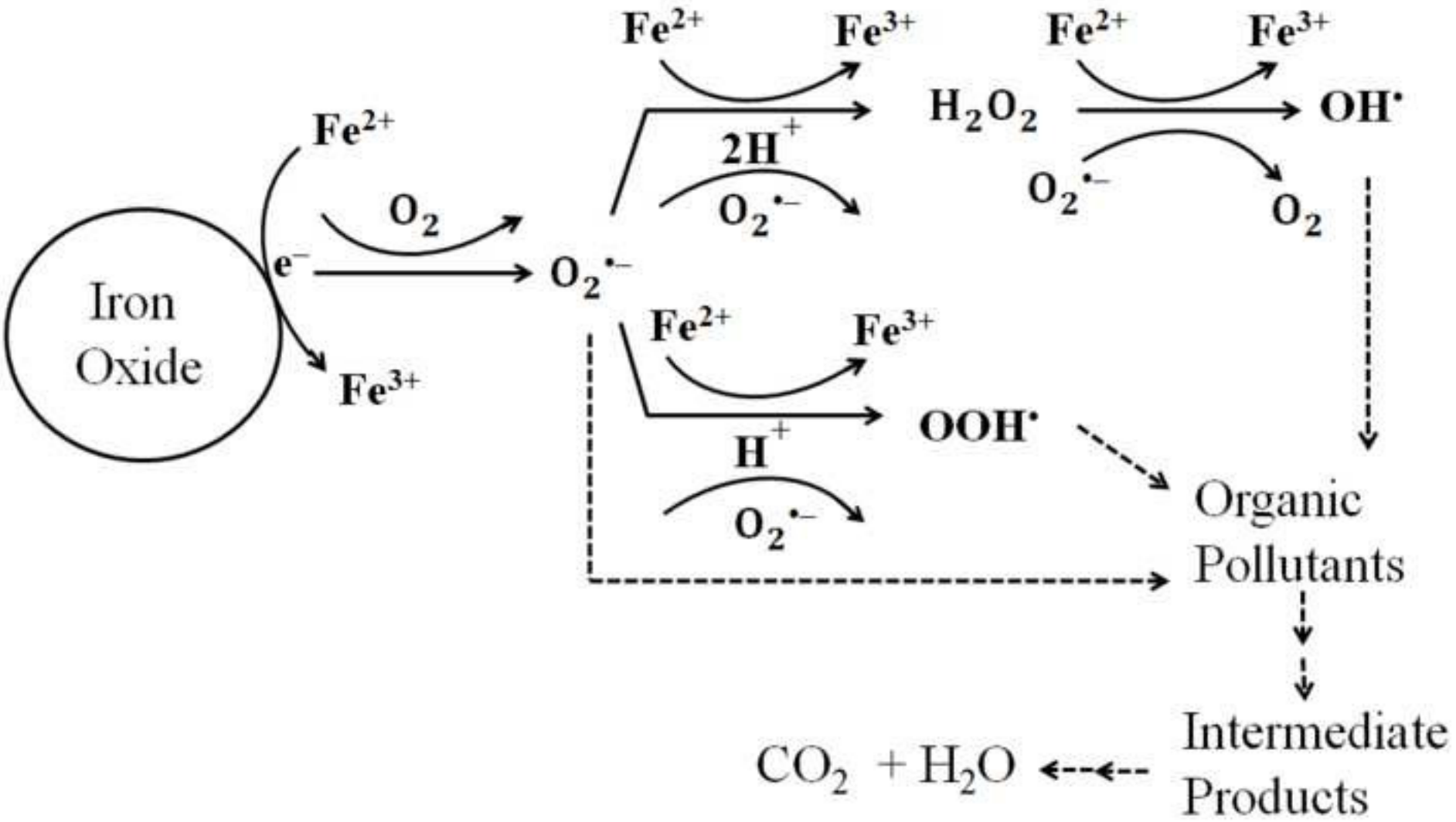

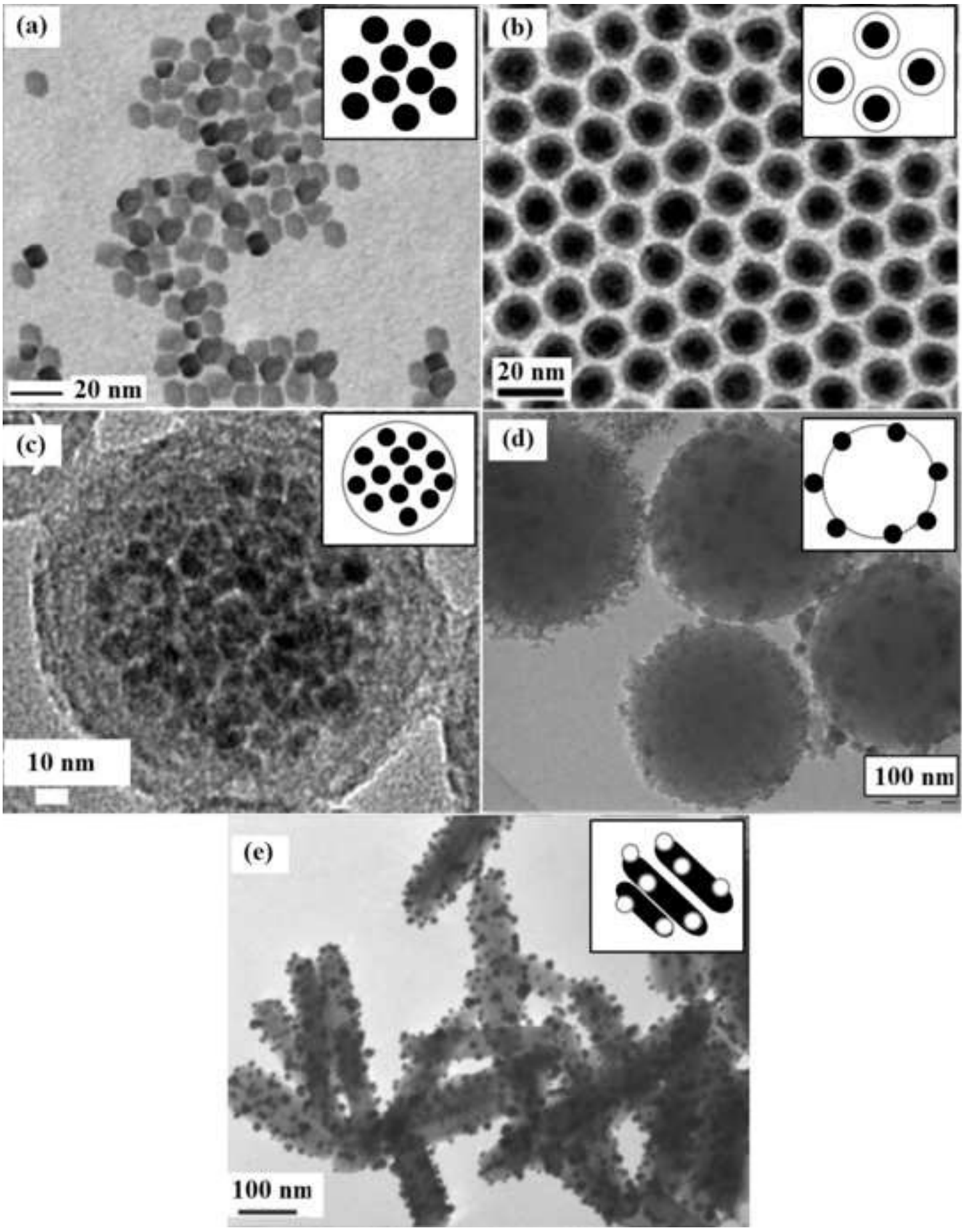

Fig. 10

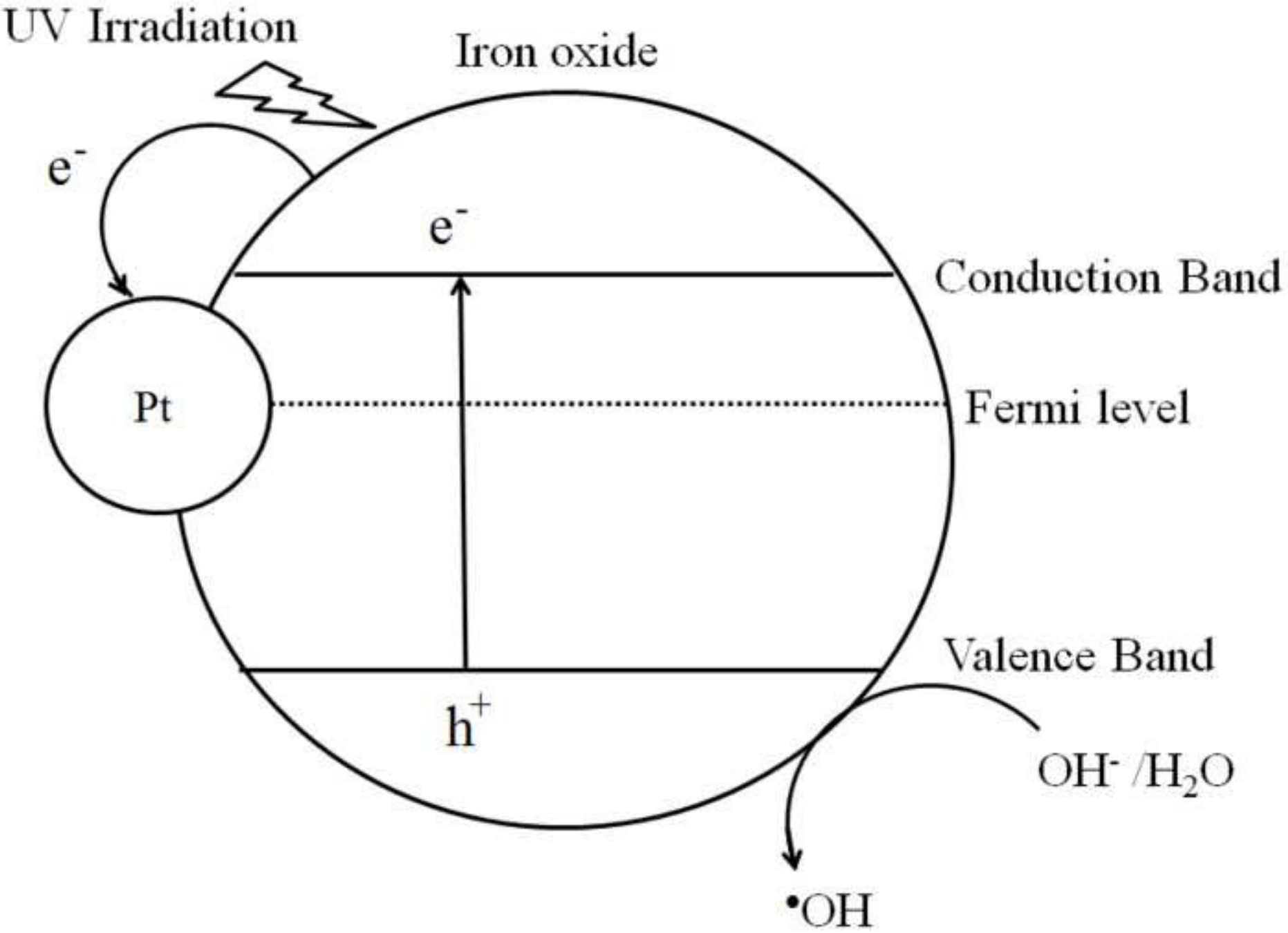

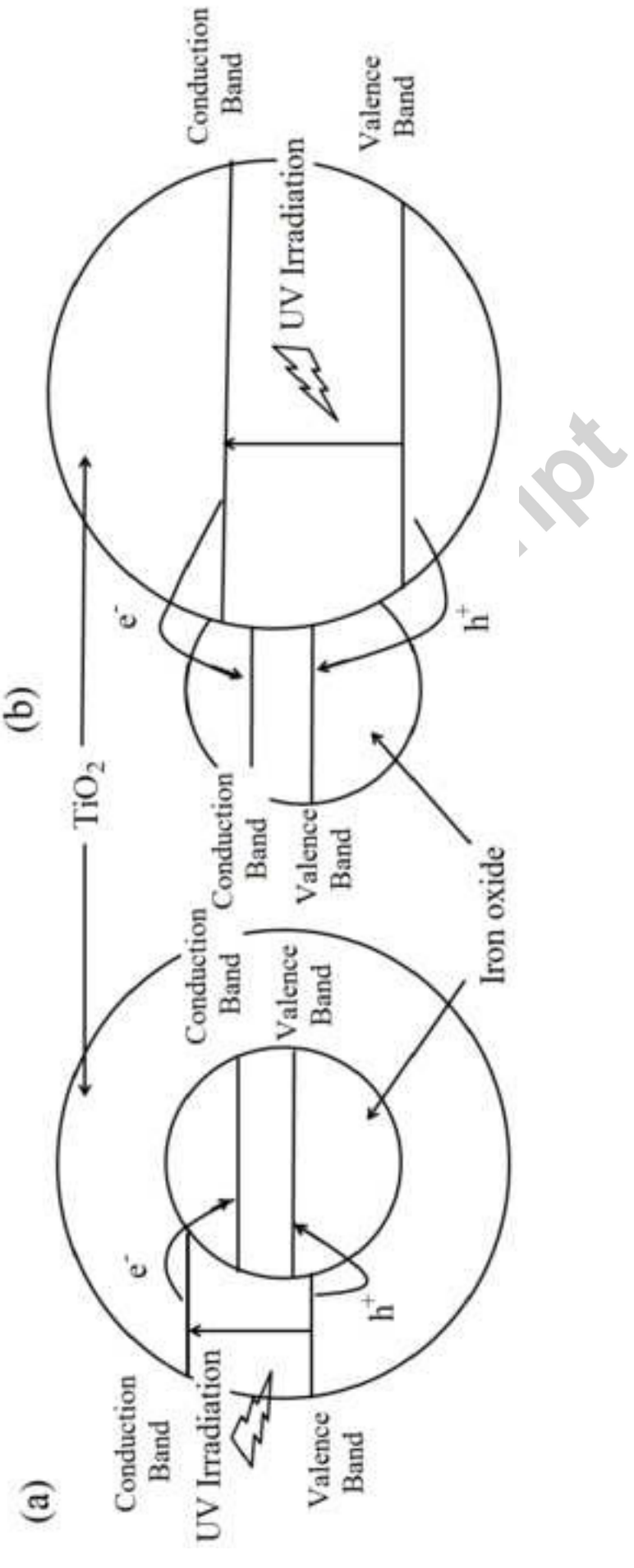

Fig. 11

Table 1: Comparison of the synthesis methods of iron oxide magnetic particles.

Methods	Reaction condition [32]	Characteristic of the obtained products [50]	Advantages	Disadvantages
Co-precipitation	Temperature: 20–90 ^{o}C Duration: Minutes Solvent: Water	Shape control: Not good Size distribution: Broad Crystallinity: Poor polydispersity Magnetization value: 20–80 emu/g [49, 51]	Simple, easy and low cost method to obtain large quantities of products	Difficult to avoid nucleation during reaction and the obtained particles have a weak magnetic response
Thermal decomposition	Temperature: 100–320 ^{o}C Duration: Hours–days Solvent: Organic compound	Shape control: Very good Size distribution: Very narrow Crystallinity: High monodispersity Magnetization value: up to 91 emu/g [52]	High quality Fe_3O_4 nanoparticles can be prepared	Require relatively high temperatures, complicated procedures and usage of multiple reagents
Solvothermal	Temperature: 140–260 ^{o}C Duration: Hours Solvent: Organic solvent/ Polyglycol	Shape control: Good Size distribution: Narrow–broad Crystallinity: High monodispersity Magnetization value: up to 108 emu/g [15]	No reducing agent or surfactant is required except for liquid polyols	Relatively slow kinetic due to the relatively low temperature used and very sensitive to the concentration of water and alkalinity
Hydrothermal	Temperature: 150–220 ^{o}C Duration: Hours–days Solvent: water-ethanol	Shape control: Very good Size distribution: Very narrow/ Narrow–broad Crystallinity: High monodispersity Magnetization value: up to 93 emu/g [53]	The use of organic reagents are waived, relatively cost-effective and high yield of products	Relatively slow kinetic due to the relatively low temperature used
Microemulsion	Temperature: 20–50 ^{o}C Duration: Hours Solvent: Organic compound	Shape control: Good Size distribution: Narrow Crystallinity: Low monodispersity Magnetization value: up to 113 emu/g [54]	The particles obtained are generally very uniform without going through any size-selection process	Large amount of solvent to synthesize appreciable amount of nanomaterials

Table 2: Fabrication and application of iron oxide-based magnetic materials as photocatalysts.

Type of catalyst	Preparation method	Magnetic properties	Details of experiment	Key findings	References
Iron oxide					
α-Fe_2O_3 nanotubes (NTs) array	Electrochemical anodization method Precursor: Pure iron foils	No related information provided.	Photoelectrocatalytic and photocatalytic degradation of 1 x10^{-6} M methylene blue dye solution. Energy source: visible light with wavelength (λ) ≥420 nm and simulated solar light (1.5G)	• α-Fe_2O_3 NTs showed a pore diameter of 40 nm, thickness of 2 μm and a minimum wall thickness of 10 nm. • The rate constant on α-Fe_2O_3 NTs was 4.7 folds higher than that on TiO_2 NTs.	Zhang et al. [2]
α-Fe_2O_3, Fe_3O_4 and γ-Fe_2O_3 micropine dendrites	Hydrothermal method and oxidation-reduction process Precursor: Potassium ferricyanide ($K_3[Fe(CN)_6]$)	No related information provided.	Photocatalytic degradation of 30 ppmv gaseous toluene. Energy source: 150 W Xe lamp	• α-Fe_2O_3 showed higher catalytic activity than the other two samples. • Phase transformation-induced crystal plane effect of α-Fe_2O_3 improved adsorption ability, quantum efficiency and diffusion speed of photo-induced electron-hole pairs into charge carrier.	Wu et al. [128]
α-Fe_2O_3 urchinlike nanostructures	Hydrothermal method Precursor: Ferric chloride hexahydrate ($FeCl_3 \cdot 6H_2O$) and tetrabutyl titanate	α-Fe_2O_3 nanostructures: M_r = 0.144 emu/g; H_c = 115 Oe at 5 K	Photocatalytic degradation of 1 x 10^{-5} M Rhodamine B. Energy source: 250 W high-pressure Hg lamp	• α-Fe_2O_3/TiO_2 nanostructures displayed higher photocatalytic activities than the as-obtained sea urchinlike hematite nanostructure.	Zeng et al. [129]
Doped iron oxide					
Gallium (Ga)-doped α-Fe_2O_3	Co-precipitation method Precursors: Iron(III) nitrate ($Fe(NO_3)_3$) and gallium nitrate ($Ga(NO_3)_3$)	No related information provided.	Photocatalytic degradation of 10 mg/L methyl orange dye solution. Energy source: 500 W high-pressure mercury lamp with a maximum emitting radiations of 365 nm and 350 W Xe lamp (simulated solar light)	• Doping Ga^{3+} into α-Fe_2O_3 increased the specific surface area, the separation efficiency of photo-induced charges and the formation rate of •OH during photocatalytic reaction process. • α-Fe_2O_3 doped with 3 % Ga possesses the best photocatalytic activity.	Xiao et al. [130]

Table 2: Continued.

Type of catalyst	Preparation method	Magnetic properties	Details of experiment	Key findings	References
Sulfur (S), nitrogen (N) co-doped α-Fe_2O_3	Co-precipitation technique Precursors: Iron(III) nitrate nonahydrate ($Fe(NO_3)_3 \cdot 9H_2O$), thiourea, urea and sodium sulfide	No related information provided.	Photo-fenton and photocatalytic degradation of 100 ppm rhodamine B dye solution. Energy source: sunlight	• S,N co-doped α-Fe_2O_3 showed a superior catalytic activity compared to the individual doping of S and N. • Co-doping of S and N formed a trap state to entrap the charge carrier, delayed the recombination process and enhanced the interaction between Fe^{3+} and H_2O_2.	Pradhan et al. [6]
Barium (Ba)-cadmium (Cd)-strontium (Sr)-titanium (Ti) doped Fe_3O_4 nanohollow spheres	Solvothermal method Precursors: $FeCl_3 \cdot 6H_2O$, strontium chloride, barium chloride, cadmium chloride, titanium (IV) tetrabutoxide ($Ti[O(CH_2)_3CH_3]_4$, TBT)	Ba-Cd-Sr-Ti doped Fe_3O_4 nanohollow spheres: M_s = 40 emu/g; M_r = 4 emu/g; H_c = 40 Oe	Photocatalytic degradation of 100 mg/L congo red dye solution. Energy source: 500 W high-pressure mercury-vapor lamp (λ = 546.8 nm)	• Ba-Cd-Sr-Ti doped Fe_3O_4 led to the red shift absorption and achieved high degradation performance. • Fe^{3+} ions acted as both electrons and holes traps. • Co-doping materials able to generate electron-hole pairs effectively and released the trapped charges.	Rahimi et al. [131]
Zinc (Zn)-doped γ-Fe_2O_3 nanoplates	Solvothermal method Precursors: $FeCl_3 \cdot 6H_2O$, Zn(Ac)2·2H2O, urea	Zn-doped γ-Fe_2O_3: M_s = 58-76 emu/g	Photocatalytic degradation of 2 x 10^{-5} M rhodamine B dye solution. Energy source: visible light irradiation from a 500 W xenon lamp with a 420 nm	• Zn doped γ-Fe_2O_3 showed higher photocatalytic activity as compared to commercial P25.	Yang et al. [132]
Metal-loaded iron oxide					
Au nanoparticles on α-Fe_2O_3 photoanodes	Spray pyrolysis Precursors: Iron(III) acetylacetonate, gold chloride ($HAuCl_4$).	No related information provided.	Photoelectrochemical water splitting. Energy source: 450W xenon lamp with an above-band gap photon flux (λ < 600 nm)	• The plasmonic light absorption of the Au nanoparticle in the surface configuration was higher than the embedded configuration and subsequent higher energy transfer to the semiconductor of α-Fe_2O_3.	Thimsen et al. [133]

Table 2: Continued.

Type of catalyst	Preparation method	Magnetic properties	Details of experiment	Key findings	References
Platinum (Pt)/α-Fe_2O_3 nanorods	Hydrothermal method followed by polyol-reduction method Precursors: $FeCl_3 \cdot 6H_2O$, chloroplatinic acid (H_2PtCl_6)	No related information provided.	Photocatalytic degradation of 20 mg/L methylene blue dye solution. Energy source: 20 W fluorescent lamp with a wavelength range of 400–760 nm	• 1.79 at. % Pt showed high photocatalytic activity as compared to pristine α-Fe_2O_3 nanorings (negligible). • Metallic Pt facilitated the separation of electron-hole pairs and inhibited recombination of the photo-generated charge carriers. • Pt acted as active centers for absorbing oxygen species and methylene blue.	Chen et al. [134]
Composite semiconductors					
Fe_3O_4/ZnO core-shell nanocomposite	Co-precipitation method followed by direct precipitation method Precursors: $FeCl_3 \cdot 3H_2O$, $FeSO_4 \cdot 7H_2O$, zinc acetate, ammonium carbonate	M_s for Fe_3O_4 and Fe_3O_4/ZnO at molar ratio of 1:30, 1:15, 1:10, 1:7.5, and 1:6 were 67.78, 5.52, 9.72, 13.67, 17.12, and 20.33 emu/g, respectively.	Photocatalytic degradation of 20 ppm methyl orange dye solution. Energy source: UV irradiation of a lamp with the powder of 30 W	• Fe_3O_4/ZnO with molar ratio of 1:10 showed the highest degradation percentage, which attributed to the largest specific surface area.	Hong et al. [135]
Fe_3O_4/WO_3 core-shell composite	solvothermal method Precursors: $FeCl_3 \cdot 3H_2O$, sodium acetate, oleic acid, ethylene glycol, tungsten hexachloride (WCl_6)	Fe_3O_4/WO_3 core-shell structures: M_s = 58 emu/g; H_c = 160 Oe	Photocatalytic degradation of 4 mg/L Rhodamine B and methylene blue dye solutions. Energy source: visible light from a 300W Xe lamp with light intensity of 28 mW/cm^2	• Fe_3O_4/WO_3 hierarchical core-shell structures showed higher photocatalytic activity than the Fe_3O_4 microspheres and the commercial WO_3 particles.	Xi et al. [104]

Table 2: Continued.

Type of catalyst	Preparation method	Magnetic properties	Details of experiment	Key findings	References
Fe_3O_4/ cadmium sulfide (CdS) nanocomposites	Polyol method followed by sonochemical method Precursors: $FeCl_3 \cdot 6H_2O$ and $CdCl_2 \cdot 2.5H_2O$	Fe_3O_4: M_s = 74 emu/g; H_c = 47 Oe Fe_3O_4/ CdS: M_s = 52 emu/g; H_c = 30 Oe	Photocatalytic degradation of 6 x 10^{-5} M methyl orange dye solution. Energy source: 100 W mercury lamp	• Fe_3O_4/CdS nanocomposites displayed fluorescence and exhibited excellent magnetic properties at room temperature. • Photodecomposition rate decreased slightly after 12 cycles and degradation rate of methyl orange was 89 % in the last usage.	Liu et al. [101]
MnO_2 nanosheet-coated Fe_3O_4 nanocomposite	Hydrothermal combined with a mild ultrasonic method Precursors: $FeCl_3 \cdot 6H_2O$, sodium citrate, potassium permanganate ($KMnO_4$)	Magnetic nanoparticles: M_s = 19.28–55.61 emu/g; H_c = 82.2–83.6 Oe Magnetic hollow nanospheres: M_s = 22.42–78.31 emu/g; H_c = 68.2–70.2 Oe	Photocatalytic degradation of 20 mg/L methylene blue dye solution. Energy source: UV-vis light (wavelength range of 350−450 nm) derived from a 250 W high-pressure mercury lamp	• MnO_2 nanosheet-coated Fe_3O_4 nanocomposite with 20 mL of $KMnO_4$ showed the best photocatalytic activity and its reusability was only decreased slightly 6.8% after 5 catalytic cycles. • The magnetization values were reduced with increasing concentration of $KMnO_4$.	Zhang et al. [136]
Encapsulation of iron oxide					
Triple-shelled $Ag/Fe_3O_4/SiO_2/TiO_2$ nanospheres	Solvothermal Precursors: $Fe(NO_3)_3 \cdot 9H_2O$, sodium acetate, $AgNO_3$, tetraethoxysilane, (3-aminopropyl)triethoxy silane	$Ag/Fe_3O_4/SiO_2/TiO_2$ nanocomposite: M_s = 13.92 emu/g	Photocatalytic degradation of 20-50 ppm methylene blue dye solution. Energy source: Xe lamp with/without a filter to cut off the light below 425 nm	• The photocatalytic acticity under Xe light irradiation was followed order of $Ag/Fe_3O_4/SiO_2/TiO_2$ (un-annealed) > P25> $Ag/Fe_3O_4/SiO_2/TiO_2$ (annealed) > $Fe_3O_4/SiO_2/TiO_2$ > TiO_2 microspheres. Meanwhile, photocatalytic behavior under visible light was $Ag/Fe_3O_4/SiO_2/TiO_2$ (unannealed) > $Fe_3O_4/SiO_2/TiO_2$ > $Ag/Fe_3O_4/SiO_2/TiO_2$ (annealed) > P25	Su et al. [137]

Table 2: Continued.

Type of catalyst	Preparation method	Magnetic properties	Details of experiment	Key findings	References
Magnetic-cored dendrimer with TiO_2	Co-precipitation, sonochemical and solvothermal methods Precursors: $FeCl_3$, iron(II) sulfate heptahydrate ($FeSO_4 \cdot 7H_2O$), ethylenediamine and titanium (IV) isopropoxide	Magnetic nanoparticles: M_s = 74.5 emu/g magnetic-cored dendrimers: M_s = 62.8 emu/g magnetic-cored dendrimers with nano-sized TiO_2: M_s = 43.4 emu/g	Photocatalytic degradation of 10 mg/L methyl orange dye solution. Energy source: Four 6 W UV-C lights with a radiant wavelength of 254 nm	• Magnetic-cored dendrimer with TiO_2 retained high photocatalytic degradation after five consecutive runs. • Magnetic-cored dendrimers with nano-sized TiO_2 able to restrain recombination of electron-hole pairs because of photo-excited electron capture in dendrimers.	Kim et al. [138]
Fe_3O_4/carbon/ silver (Ag) composites	Solvothermal Precursors: $FeCl_3 \cdot 6H_2O$, sodium lauryl sulfate, sodium acetate, glucose and silver nitrate ($AgNO_3$)	Fe_3O_4: M_s = 62.5 emu/g Fe_3O_4/carbon: M_s = 32.3 emu/g Fe_3O_4/carbon/Ag composites: M_s = 31.6 emu/g	Photocatalytic degradation of 10 mg/L neutral red dye solution. Energy source: visible light from a 30 W xenon lamp (the wavelength was 400–700 nm)	• Fe_3O_4/carbon/Ag composites possess the highest photocatalytic activity.	Liang et al. [139]
Bismuth tungstate (Bi_2WO_6)/carbon/Fe_3O_4 microspheres	Solvothermal, hydrothermal and sonochemical Precursors: $FeCl_3 \cdot 6H_2O$, glucose and bismuth(III) nitrate pentahydrate	Fe_3O_4 microspheres: M_s = 37.4 emu/g Bi_2WO_6/carbon/Fe_3O_4 microspheres: M_s = 81.9 emu/g	Photocatalytic degradation of 20 mg/L phenol solution. Energy source: 500W xenon lamp with a cut-off filter of ($\lambda \geq 420$ nm)	• Activated carbon layer acted as an essential "bond" for combining two materials i.e. Bi^{3+} ions could be adsorbed by the oxidized carbon layer (–COO− group). • Bi_2WO_6/carbon/Fe_3O_4 could be easily recovered by a magnet, exhibited high catalytic activity with the assistance of H_2O_2.	Zhang et al. [140]

Table 3: Band gap energies and energy levels of conduction band and valence band with respect to AVS for various semiconductors [156].

Semiconductor	Band gap energy (eV)	Conduction band (V)	Valence band (V)
TiO_2 (anatase)	3.20	-4.21	-7.41
ZnO	3.20	-4.19	-7.39
SnO_2	3.50	-4.50	-8.00
WO_3	2.70	-5.24	-7.94
FeO	2.40	-4.33	-6.73
Fe_3O_4	0.10	-5.73	-5.83
Fe_2O_3	2.20	-4.78	-6.98
CdS	2.40	-3.98	-6.38